Sensitive High Resolution Ion MicroProbe – Stable Isotope (SHRIMP-SI) analysis of water in silicate glasses and nominally anhydrous reference minerals

Journal:	*Journal of Analytical Atomic Spectrometry*
Manuscript ID:	JA-ART-02-2015-000047.R1
Article Type:	Paper
Date Submitted by the Author:	15-Apr-2015
Complete List of Authors:	Turner, Michael; Macquarie University, Earth and Planetary Sciences Ireland, Trevor; Australian National University, Research School of Earth Sciences Hermann, Joerg; Australian National University, Research School of Earth Sciences Padron-Navarta, Jose Alberto; University of Montpellier and CNRS, Geoscience Montpellier Hauri, Erik; Carnegie Institution of Washington, Department of Terrestrial Magnetism Holden, Peter; Australian National University, Research School of Earth Sciences Turner, Simon; Macquarie University, Earth and Planetary Sciences

SCHOLARONE™
Manuscripts

1 **Sensitive High Resolution Ion MicroProbe – Stable Isotope**

2 **(SHRIMP-SI) analysis of water in silicate glasses and**

3 **nominally anhydrous reference minerals**

4

5 Michael Turner,[a] Trevor Ireland,[b] Joerg Hermann,[b] Peter Holden,[b] José Alberto Padrón-

6 Navarta,[b,c] Erik H. Hauri,[d] Simon Turner [a]

7

8 Low-level water measurements of geological materials are fundamental in understanding the volatile

9 inventories of the Earth from the mantle to crustal reservoirs. Here we describe the development of

10 microanalytical techniques using the new SHRIMP SI ion microprobe to measure the abundances of

11 OH^- (as a proxy for water) in volcanic glass and nominally anhydrous minerals (NAMs). Samples were

12 first analysed at the Carnegie Institute of Washington on their Cameca ims-6f with calibrations based

13 on previous FTIR analyses. SHRIMP SI is a large geometry ion microprobe and is currently mainly

14 used for O and S isotope analyses. The analytical protocol used here incorporates multiple collection of

15 $^{16}O^-$ and $^{16}O^1H^-$ allowing rapid measurements. A single calibration line incorporating all glasses and

16 NAMs for the SHRIMP SI allows calibration of $^{16}O^1H^-/^{16}O^-$ to H_2O over a wide range in concentration

17 (50 to 15,000 ppm H_2O). This calibration line has around a 10% uncertainty, which appears to be

18 limited only by sample heterogeneity. The current background for SHRIMP analysis is between 20-40

19 ppm but this is expected to improve with improved pumping on the source chamber.

20

21 A current limitation to water analysis of NAM samples, by any technique, is having a range of standard

22 materials to enable OH^- calibration to absolute H_2O concentrations. Data are presented for 7 NAM

23 samples (2 olivines, 2 orthopyroxenes and 3 clinopyroxenes) that appear to be promising as potential

24 standards for international laboratory H_2O measurements. These NAM samples have been analysed

25 and characterised here by SHRIMP SI, FTIR, EMP and the Cameca ims-6f ion microprobe at CIW.

26 Four of these samples have previously been measured by manometry to determine absolute H_2O

27 concentrations.

28   **Introduction**

29

30   The analysis of water to low levels in glass inclusions of volcanic phenocrysts and, in recent years,

31   within the crystal structure of nominally anhydrous minerals (NAM), has facilitated a better

32   understanding of how water is recycled between the Earth's mantle, crust, and hydrosphere. [1,2,3,4,5]

33

34   Secondary ion mass spectrometry (SIMS) analysis is routinely used to measure water concentrations in

35   melt inclusions of volcanic phenocrysts, [5,6] as well as volatile concentrations in NAM. [7,8,9,10,11] Most of

36   this work is carried out on small geometry ion microprobes such as the Cameca ims 3f-7f models,

37   where the small source chamber volume, and hence minimal surface area, allows vacuum pressures of

38   the order of 5 $\square$ 10^{-10} mbar to be obtained. It is well noted that low vacuum pressures are essential in

39   obtaining low analytical backgrounds of water because water is a persistent species in vacuum to very

40   low pressures and in optimal circumstances water levels should be quantified down to sub 10 ppm

41   levels. [7] In contrast, large magnetic sector ion microprobes such as SHRIMP (Sensitive High

42   Resolution Ion MicroProbe) or Cameca 1280 have generally not been used for water measurements at

43   low abundances. In part this is due to the larger source chamber volume, which directly affects the

44   signal from desorbing-adsorbing water molecules from the target surface. Furthermore, the large mass

45   analyzers are difficult to tune for measurement of the H species (H^- or H^+) because of the long total

46   beam paths and interactions with the terrestrial magnetic field and/or other stray magnetic fields.

47   However, these large magnetic sector mass spectrometers have much higher inherent sensitivity at high

48   mass resolution and so pursuit of a viable analytical technique for water has advantages in terms of

49   signal strength at low water concentration.

50

51   Many of the ion microprobes being used for water analysis are dedicated to this task. This is to allow

52   optimal vacuum conditions to be maintained. To this end, metal (Indium) mounts are typically used

53   that present low inherent water to the vacuum system. On the other hand, epoxy mounts commonly

54   used for mounting small crystal grains have high inherent volatiles. Currently, SHRIMP SI is being

55   used mainly for stable isotope analysis. This involves introduction of a variety of glass and epoxy

56   mounts, which can therefore adversely affect the vacuum. Part of this work is to understand how we

57   can increase the versatility of SHRIMP SI to allow a range of mounting materials into the vacuum

58   system while still allowing us to do low level water analysis.

59

60   Fourier Transform Infra-Red spectroscopy (FTIR) is the most common technique used to determine

61   water concentrations of glasses and minerals. Samples to be analysed by this technique need to be of

62   such a dimension that allows wafers to be manufactured, typically around 100 μm thick and doubly

63   polished. The analytical area needs to be inclusion free and preferably be greater than 80 x 80 μm to

64   allow precise absorbance measurements, depending on the thickness of the sample and for the FTIR

65   analysis of water in small sample sets of anisotropic minerals, the samples need to be optically

66   orientated. [12] Microanalysis of OH-stretching vibrations and molecular H_2O in glasses or

67   crystallographic OH^- in minerals by FTIR can resolve water concentrations to less than 5 ppm in

68   optimal circumstances using appropriate calibrations.

69

70   SIMS and FTIR methodologies are based on comparisons with reference materials and these require

71   measurement of their absolute water concentrations. Few current reference materials for SIMS and

72   FTIR have been independently measured and much of normalisation for water analysis is based on

73   circular comparisons between SIMS and FTIR. As such there is a need for homogeneous standard

74   materials of sufficient quantities that can be used routinely for calibration of both SIMS and FTIR.

75   Reference materials are required to be homogeneous both on the analytical scale of SIMS and FTIR

76   analysis, and on the scale of chips that could be distributed between laboratories.

77

78   In this paper, we present the first H_2O measurements of natural glasses and silicate minerals using the

79   large geometry ion microprobe SHRIMP SI and compare them directly to measurements made on the

80   Carnegie Institution of Washington (CIW) Cameca ims-6f ion microprobe. These analyses are also

81   compared to new FTIR measurements made at the Australian National University (ANU), as well as

82   published FTIR and manometry measurements (e.g. [13]). The resulting database of SIMS and FTIR H_2O

83   analyses on geological materials are then used to discuss and make recommendations on the use of

84   glass and NAM standards.

85

86   **Material and methods**

87

Samples

89 Six natural basaltic glasses and seven NAM samples (consisting of two olivine, two orthopyroxene and

90 three clinopyroxene mineral samples) were selected for analysis.

91

92 1. BASALTIC GLASSES

93 Naturally quenched basaltic glasses were obtained from the Fonualei Spreading Centre (ND-60, ND-

94 61), Mangatolo Triple Junction (ND70, ND69) and Manus Basin (24.1, 36.4). All glass samples have

95 been characterised for major and trace element geochemistry in the studies of Keller et al. [14] for

96 Fonualei and Mangatolo samples and Sinton et al. [15] for the Manus Basin samples. Our ND60, ND61,

97 ND69 and ND70 glass fragments were sourced from Richard Arculus (Australian National University)

98 and are subsamples from ocean-dredged rocks chosen as glass standards for the Cameca ims-6f facility

99 at CIW (i.e., ND-60-01, ND70-01). [16,17] ND-60, ND-61 and ND-69 samples used in this study

100 contained quench inclusions of plagioclase. These were avoided in all types of analyses.

101

102 2. NOMINALLY ANHYDROUS MINERALS

103 Two olivine and five pyroxene samples were selected for analysis. Othropyroxene KBH-1 opx, an

104 aluminous enstatite from Kilbourne Hole, New Mexico and PMR-53, an augite megacryst from

105 Premier Mine, South Africa have had their water contents determined by manometry (KBH-1 opx: 217

106 ppm H_2O; PMR-53: 268 ppm H_2O). [13] These samples were used by Bell et al. [13] to determine

107 integrated absorption coefficients for O-H bonds in FTIR spectra of pyroxene minerals. Similarly,

108 clinopyroxene KBH cpx, also from Kilbourne Hole, New Mexico, was used in the FTIR study of Bell

109 and Rossman [1] and has a manometry determined H_2O content of 530 ppm.[1] In addition, gem quality

110 natural samples of pyroxene and olivine were obtained from Russia, Pakistan, Tanzania and USA. The

111 Russian Cr-diopside is from an unidentified location in Russia, but does appear to be similar to the

112 Russian Cr-diopside used in the studies of Shannon et al., [18] Ingrin et al. [19,20] and sample 62047-70B of

113 the recent Mosenfelder and Rossman study. [11] The Pakistani olivine is from a pocket or vein located in

114 the shear zones of serpentinised dunitic rocks of Sapat, Kaghan Valley, Kohistan arc, Pakistan. Gem-

115 quality Pakistani olivine was obtained from the same location as was used in the studies of Gose et al.

116 [21,22] and Kovacs et al. [23] It was noted that some Pakistani olivine crystals contained small inclusions of

117   serpentine and/or needles of boron-bearing fibrous minerals (likely ludwigite-vonsenite, see Bouilhol *et*

118   *al.* [24]). These inclusions were avoided in all geochemical and infrared spectroscopy analyses of this

119   study. The Tanzania orthopyroxene is likely to be similar to the enstatite from Dodoma, Tanzania used

120   by Beran and Zemann [25] and to the sample JLM46 in the recent study of Mosenfelder and Rossman. [10]

121   San Carlos olivine samples are derived from xenoliths found within the Pliocene San Carlos alkali

122   basalt lava flow Arizona, U.S.A. We used two different samples of San Carlos olivine. San Carlos 1 is

123   a mm-sized cube of light green colour that was measured with EMP, IR and SIMS and appears similar

124   to those typically used for SIMS and FTIR studies. [26,27] Additionally, the polarized IR spectra of an

125   unusually large crystal (>5 mm) with slightly darker colour (San Carlos 2) was analysed and compared

126   to those typically used for SIMS and FTIR studies. [26,27]

127

128   **Sample preparation**

129   The quality of the vacuum in the sample chamber is one of the most dominant factors that controls the

130   background for measurements of water by SIMS. Epoxy mounts continuously out-gas hydrocarbons

131   and water under vacuum and are therefore one of the largest contributors to the mass spectrometer

132   vacuum and hence $^{16}O^1H^-$ background measurements. In order to eliminate the epoxy contribution,

133   glasses and silicates were first polished in a Crystalbond embedding medium, then extracted with

134   acetone before being pressed into indium one-inch ion probe mounts (c.f. [6]). A single indium mount

135   was made that contained fragments of each of the samples. The mount was photographed in reflective

136   light and was then gold coated for SIMS analysis. After SIMS analysis, the mounts were lightly

137   polished with Al paste and carbon coated for electron-microprobe analysis.

138

139   Fragments of some of the same mineral and glass samples used for the ion probe study were analysed

140   by FTIR. Glass fragments were cut into wafers of around 3x3 mm, approximately 100 μm thick, and

141   double polished using diamond and alumina compound. NAM grains were cut into tabular rhomboids

142   that measured between 1x1 mm and 5x5 mm after final polish. The olivine and orthopyroxene samples

143   were cut approximately parallel to the three crystallographic axes of the orthorhombic minerals before

144   being polished for FTIR analysis. The gem Cr-diopside was cut along three perpendicular sections that

145   were dictated by the cleavage of the pyroxene.

146

147 **Experimental Techniques**

148

149 1. SENSITIVE HIGH RESOLUTION ION MICROPROBE – STABLE ISOTOPE (SHRIMP SI)

150

151 SHRIMP SI is a secondary ion mass spectrometer configured as an ion microprobe (Fig. 1) [28] and is

152 one of three SHRIMP instruments housed in the Research School of Earth Sciences at The Australian

153 National University. SHRIMP SI was specifically designed for light isotope analysis, but it also has a

154 number of vacuum controls that enhance its capability for water analysis compared with other

155 SHRIMP instruments.

156

157 The main changes for SHRIMP SI compared to previous generation SHRIMP instruments are in and

158 around the source chamber with a goal of improving the vacuum. The SHRIMP SI source chamber is

159 machined out of a single piece of 316-grade stainless steel with differential pumping to the primary

160 column, to the quadrupole triplet system, and to the electron column (Fig. 1). Internal stage motors

161 have been replaced by a bellows system with external drives. The vacuum interlock consists of a two-

162 stage system with the inner lock having a UV lamp to enhance water excitation from the sample

163 surface.

164

165 The source chamber is pumped with a Varian 300 l/s ion pump with a Ti sublimation unit. This

166 pumping system was chosen for its low ultimate vacuum pressure, and lack of mechanical vibration

167 that could affect sample stability. During analyses,, the sample chamber vacuum pressure was

168 measured to be between 7 and 9 x 10^{-9} mbar as indicated by an ion gauge in the source chamber, while

169 the current passing through the ion pump is consistent with pressures around 1-3 x 10^{-9} mbar.

170

171 The primary ion beam for SHRIMP SI is Cs^+ that is generated in a Kimball Physics model IGS-4 ion

172 gun with Cs^+ zeolite as the emitter. Cs^+ ions are initially focused through an accelerating potential of 5

173 kV in the gun. The Cs^+ beam is focused to the Kohler aperture, which is located at the focal point of the

174 final einzel lens. This lens operates as an immersion lens to accelerate the beam to sample potential

175 (providing an additional 10 keV giving a total beam energy at the target of 15 keV), and to demagnify

176   the Kohler aperture by a factor of 10 on to the sample surface. Thus a 200 µm Kohler lens produces a

177   20 µm "spot".

178

179   Sputtering with a primary Cs^+ beam results in charge build up owing to the delivery of a positively

180   charged primary beam, and extraction of negative secondary ions (and electrons). In order to neutralise

181   charging, electrons are focused from the Kimball electron gun (model ELG-2) to the surface at a 45°

182   incidence angle and with a final energy of around 1.5 keV. The electron column operates with a quasi-

183   Kohler illumination system in order to improve the uniformity of illumination.

184

185   Negative secondary ions are accelerated from the -10 kV sample potential via an initial 800V potential

186   difference to the extraction plate. A feature of the SHRIMP SI design is a vertical and horizontal beam-

187   steering capability on the extraction plate. The beam is then accelerated to real ground and beam

188   transmission is maximized to the source slit with a symmetric (circular aperture) einzel lens system

189   followed by the standard quadrupole-triplet lens system used on SHRIMP II.

190

191   SHRIMP SI uses the same forward-geometry as SHRIMP-II instruments with a double-focusing mass

192   analyzer design [29] to enable high mass resolution (5500 M/ΔM at 10% peak width for 100 µm entrance

193   and exit slits) while maintaining high sensitivity through a physically large mass spectrometer (magnet

194   turning radius of 1000 mm). SHRIMP-SI was originally designed with a three-head multiple collector;

195   ions can be measured in Faraday cups, or with interchangeable electron multipliers. The multiple

196   collector has since been modified to incorporate a fourth detector for measuring ^{33}S in four-sulfur

197   isotope measurements. [30] During analysis the pressure in the mass analyser and collector is in the range

198   of 1 to 3 x 10^{-8} mbars. At these pressures only minor ion scattering is produced and therefore there is

199   minimal contribution to the $^{16}O^1H^-$ background..

200

201   The multiple collector was configured to allow simultaneous measurement of ^{16}O and $^{16}O^1H^-$. For

202    $^{16}O^1H^-$, a 100 µm collector slit was used to achieve high mass resolution (5,500 M/ΔM) sufficient for

203   full resolution of ^{17}O and $^{16}O^1H^-$ (Fig. 2). For ^{16}O on the low mass head a 400 µm collector slit was

204   used (ca. 1250 M/ΔM). The low resolution provides a broad flat top peak for ^{16}O so any differential

205   movement of ^{16}O from $^{16}O^1H^-$ does not affect the ^{16}O beam intensity. During data acquisition, the

206     $^{16}O^1H^-$ peak is centred, or if $^{16}O^1H^-$ is very low, ^{17}O is centred followed by a peak jump to $^{16}O^1H^-$.

207

208   SHRIMP analyses have been performed with $^{16}O^1H^-/^{16}O^-$ in order to allow the water concentration to

209   be assessed with a static magnet position in multiple collection mode. This mode facilitates data

210   collection and analysis with no need for time interpolation of the signals. There is potentially some

211   ambiguity in the O^- signal in that some of that signal could be sourced from molecular break up of

212     $^{16}O^1H^-$ during sputtering. However this is expected to be a very small component because all of the

213   targets are silicates with large $^{16}O^-$ signals. Furthermore it is essentially removed by the calibration

214   provided there is a consistent dissociation of $^{16}O^1H^-$ at differing concentrations.

215

216   Prior to insertion in to SHRIMP SI, the mount contained in the mount holder was placed in a vacuum

217   oven overnight, and the mount was pumped down in the sample lock for 24 hours prior to analysis. A

218   spot size of 30 μm was used for analysis. The primary beam was first rastered over the spot area for

219   120 seconds to remove gold and any surface contamination. The beam was then stabilised for 60

220   seconds prior to an automated beam alignment procedure. Five static analyses of $^{16}O^1H^-/^{16}O^-$ were

221   acquired, each consisting of ten sequential 2-second integrations, with a total time of analysis

222   (including background) of 320 seconds. Measurement errors less than 5% were taken as indicative of a

223   homogenous water concentration within the analysis. Analyses that showed heterogeneity with depth

224   within a single sputter crater were discarded.

225

226   Determining the absolute sensitivity for water analyses on SHRIMP SI is not straightforward because

227   the electron beam signal dominates over the primary beam and secondary ion beam. Our best estimate

228   for the primary beam intensity used in this work is around 5 nA and is similar to that reported by Ickert

229   *et al.* [31] for oxygen isotope analysis.[31] Sensitivity of $^{16}O^1H^-$ analyses on the SHRIMP SI is estimated at

230   170 c/s/ppm H_2O yielding a sensitivity of approximately ca. 35 cps/ppm H_2O/nA. This is substantially

231   higher than the sensitivity reported for the CIW Cameca 6f (2 cps/ppm H_2O/nA)[6] and is in accord with

232   the transmission estimated from Ti isotope analysis.[32,33]

233

234   2. CAMECA IMS-6F

235

236   Methods employed to measure the concentrations of water with the Cameca ims-6f ion microscope at

237   the Carnegie Institution of Washington were similar to those developed for the micro-analysis of trace

238   concentrations of volatiles in glasses and NAMs by Hauri *et al.* [6,8] and Koga *et al.* [7] Pressure in the ion

239   probe sample chamber was $< 8 \times 10^{-10}$ mbar during all analyses. Background limits (<10 ppm H_2O)

240   were determined by the repeated analysis of synthetic anhydrous forsterite and anhydrous quartz

241   (Suprasil 3002, 1 ppm H_2O, available from Heraeus Quarzglas) located in each sample mount. The

242   background of H_2O is relatively minor compared to all glasses and most NAM analyses studied here

243   (with the exception of San Carlos olivine) and therefore no background correction was made. Before

244   each analysis, the secondary ion images of $^{16}O^1H^-$ were projected on to the channel plate in ion

245   microscope mode. This helped to avoid inclusions and cracks, which appear as bright features on the

246   projected image. After each beam spot was carefully examined, the field aperture was inserted to

247   permit transmission of ions only from the central 8 μm of the 20 μm beam crater, thus avoiding

248   transmission of $^{16}O^1H^-$ from the edge of the sputter crater and the surface of the sample. The use of this

249   small field aperture reduces the transmission of ions and thus the sensitivity compared with the

250   SHRIMP SI, but is crucial for obtaining low detection limits. Rastering of the primary beam over a 50

251   μm by 50 μm area for 120 seconds was also performed to remove any surface contamination prior to

252   each analysis. Water analyses are based on the $^{16}O^1H^-/^{30}Si^-$ ratio measured through cyclically peak-

253   stepping the magnet.

254

255   A range of basaltic glasses and NAM standards are used by CIW to define calibration curves of H_2O

256   contents from $^{16}O^1H^-/^{30}Si^-$. [6,7,8,17] ND-glasses as well as PMR-53 cpx and KBH-opx samples described

257   here are used to constrain the calibration curves for glass, clinopyroxene and orthopyroxene,

258   respectively.

259

260   3. FOURIER TRANSFORM INFRARED SPECTROSCOPY

261

262   Fourier Transform infrared (FTIR) spectroscopy analysis was conducted at the Research School of

263   Earth Sciences at The Australian National University, using a Bruker IFS28 spectrometer coupled to a

264   Hyperion 1000 microscope that is equipped with a nitrogen-cooled MCT detector. The sample stage is

265   housed in a Perspex chamber that is continuously flushed with dry air in order to suppress the

266   background of atmospheric water. Doubly polished glass wafers were investigated with unpolarised

267   transmission FTIR using a 50-100 μm square aperture. The glasses were incrementally thinned to

268   optimise the intensity of the absorption for the 3570 cm-1^{-1} band. The thickness of the samples was

269   determined with a Mitutoyo mechanical device, which is accurate to 3-4 μm and were found to be

270   between 80 and 200 μm thick. The gem olivine and orthopyroxene samples were analysed with

271   polarised IR light (KRS 5 polarizer) along the three crystallographic axes whereas the clinopyroxene

272   was analysed along three perpendicular axes that are close in orientation to the crystallographic axes.

273   The spectra were acquired in the range of 5500 to 600 cm^{-1} as the average of 64-128 scans with a

274   resolution of 4 cm^{-1}. The atmospheric compensation tool from the OPUS® software was applied to all

275   spectra to minimise absorption bands related to atmospheric water. The background correction was

276   implemented by the interactive concave rubber band correction with 64 baseline points and three

277   iterations of the OPUS® software for olivine and glasses. For pyroxenes, the background was corrected

278   using a manual spline fit as described by Mosenfelder and Rossman [10,11] (see Supplementary file A1

279   for raw and baseline corrected spectra for olivine and pyroxenes measured in this work).

280

281   4. ELECTRON MICROPROBE

282

283   Mineral and glass samples were analysed on a Cameca SX100 electron microprobe in the Geochemical

284   Analysis Unit at Macquarie University, Australia. An accelerating voltage of 15 keV was used with a

285   focused beam current of 20 nA. A counting time of 10 seconds was assigned to both peak and

286   background measurements. Spectrometer calibration was achieved using the following standards: albite

287   (Na), hematite (Fe), kyanite (Al), olivine (Mg), chromium (Cr), spessartine garnet (Mn), orthoclase (K),

288   wollastonite (Ca, Si) and rutile (Ti).

289

290   **Results**

291

292   **Electron microprobe**

293

294 Compositions for both the basaltic glasses and mineral samples analysed in this study are presented in

295 Table 1. Replicates (n=7) show that all grains are relatively homogenous with standard deviations for

296 major elements in each sample typically being less than 1 % (1 sigma S.D; Table 1). Major element

297 compositions for many of the NAMs are similar to those in previously published studies on these

298 minerals (PMR-53 cpx, KBH-opx: [13] KBH-cpx: [1] Rus Cr-diop: [19,20] Tan-opx: [25]). The Pakistani olivine

299 sample with a Mg# of 95 has a higher MgO and lower FeO^t (Table 1) than the grain analyses in the

300 Gose et al. [22] study and is situated at the upper end of the range of Mg# (89-97) reported by Bouilhol et

301 al. [24]

302

303 **Infrared Spectroscopy – glass samples**

304

305 The glass samples are characterised by a large broad absorption band at 3700-2800 cm^{-1} (Fig. 3) and a

306 smaller band at 1630 cm^{-1}. The broad band is attributed to the combination of molecular water (H_2O)

307 that can fill in larger cavities in the silicate network of glasses and OH^- that is strongly associated with

308 non-bridging oxygen. [34,35,36] The smaller band at 1630 cm^{-1} is attributed to molecular water alone. The

309 linear absorptions at 3370 cm^{-1} and at 1630 cm^{-1} combined with the extinction coefficients for Fe-

310 bearing andesites from Mandeville et al., [37] were used to quantify the total and molecular water

311 contents, respectively (Table 2 and 3). Typically 10 analyses were performed on each glass sample.

312 The standard deviation of these multiple analyses varies from 0.5-3%. Combined with an uncertainty of

313 2-5% in the thickness of the samples and 5% uncertainty in the density of the glasses the total

314 uncertainty on water contents is 5.5-7.7% when the individual uncertainties are added in quadrature.

315

316 **Infrared Spectroscopy – NAM samples**

317

318 Orientated polarised FTIR analyses of the Russian Cr-diopside (Rus Cr-diop), Pakistani olivine (Pak

319 ol), Tanzanian orthopyroxene (Tan opx) and San Carlos olivine (San Carlos) were undertaken and the

320 results are shown in Fig. 4. The position of the several hydroxyl-stretching bands for individual

321 samples is also given in Fig. 4. Tan opx shows two groups of bands which are highly polarized along

322 the g optical axis (corresponding to the c-axis for orthopyroxene), the most intense ones are located

323 between 3400 and 3560 cm^{-1}, whereas broad bands are found in the range from ~2800-3400 cm^{-1}. Rus

324 Cr-diop shows two main bands at 3646 and 3430 cm^{-1} with similar absorbances close to □ and □

325 optical axes. Band position and degree of polarization for Tan opx and Rus Cr-diop are similar to those

326 commonly found in pyroxenes. [10,11] Despite the low water content the IR spectra for San Carlos-2 is

327 exceptionally well resolved in the large investigated sample (6.34 x 6.45 x 7.89 mm). IR spectra for

328 San Carlos olivine is considered to be representative of the upper mantle. It is strongly polarized along

329 the □ direction (a-axis) being the two main bands located at 3572 and 3525 cm^{-1}. OH-stretching bands

330 corresponding to trivalent substitution (ca. 3350 cm^{-1}, Berry et al. [38]) are lacking. In the smaller, mm-

331 sized cube no clear IR absorbance could be observed. Pak olivine shows a particularly unusual IR

332 spectra with maxima in absorbances along the □ and b optical axes. Band position and polarization

333 measured in Pak olivine is similar to the ones reported by Ingrin et al. [39] Kovács et al. [23] Gose et al. [22]

334 The recent study of Ingrin et al. [39] showed that the OH-stretching bands of the Pakistani olivine at

335 approximately 3700 and 3598 cm^{-1} are associated with B-H coupled substitution and that these peaks

336 are superimposed on $(4H)_{si}$ defects that result in bands at 3612, 3580 and 3566 cm^{-1} as well as the broad

337 OH-stretching band associated with interstitial OH$^-$ at 3549 and 3568 cm^{-1}. The sample that we

338 analysed is missing the relatively minor OH-stretching band associated with B-H at 3521 cm^{-1}. All

339 investigated samples are free of signals from hydrous inclusions (such as serpentine or amphiboles).

340

341 The concentrations of H_2O in NAMs were quantified combining the total integrated absorption of

342 bands in the 3750 – 2800 cm^{-1} region (see notes in Table 4, for details of the integration range for

343 different minerals), the density, thickness of the samples and specific absorption coefficients. The total

344 integrated absorption (Abs_{tot}) was obtained by adding the polarized measurements along the three

345 crystallographic axes (orthopyroxene, olivine) or three perpendicular orientations (clinopyroxene). The

346 absorption coefficient of Bell et al. [13] for orthopyroxenes (k = 0.067; H_2O (ppm wt) = k x Abs_{tot}

347 (integrated per cm)) and clinopyroxene (k = 0.141) were used here to be consistent with study of Koga

348 et al. [7] For olivine the absorption coefficient (k = 0.188) from Bell et al. [40] is given in Table 4 and for

349 the Pakistani olivine also the absorbtion coefficient (k = 0.57) of Kovács et al. [23] was used because

350 unlike the other NAMs studied here, there is a large difference between the FTIR (using Bell et al. [40]

351 calibration) and ion-probe water contents (based on the calibrated analysis from the Cameca ims 6f;

352 Table 4). The Pakistani olivine is from hydrothermal veins of serpentinised dunitic rocks whereas the

353 samples used in the Bell et al. [40] study are from pressure and temperature conditions similar to the

354   mantle environment. The use of the Bell *et al.* [40] absorption coefficient for the FTIR calibration is

355   therefore not necessarily valid for the Pakistani olivine. Ingrin *et al.* [39] showed that the proposed

356   absorption coefficient from Kovacs *et al.* [23] of 0.57 ± 0.04 is better suited for the Pakistani olivine than

357   the generic absorption coefficient of 0.188 ± 0.012 determined by Bell *et al.* [40] Encouragingly by using

358   the Kovacs *et al.* [23] absorption coefficient the calculated water content of the Pakistani olivine from our

359   FTIR analyses is almost identical to that measured by CIW ion-probe (Table 4). The error on the water

360   content has been determined by adding in quadrature the uncertainty in thickness (5 %), the total

361   absorbance (5 %) and the absorption coefficient (10 %).

362

363   **Ion probe analyses**

364

365   A subset of ND-glasses as well as fragments of PMR-53 cpx and KBH-opx are used as standards on

366   the CIW Cameca ims-6f to constrain the calibration curves for glass, clinopyroxene and orthopyroxene,

367   respectively. H_2O contents of the samples have been determined using the calibration curves based on

368   previous FTIR measurements and are presented here for comparison (Table 2). Estimated water

369   contents for the basaltic glasses and pyroxene grains are similar to those found by FTIR in this study

370   (Table 2). The errors associated with these estimates are approximately 10 % for glass and 20 % for

371   olivine and pyroxene. [7]

372

373   Cameca ims-6f H_2O data are plotted against the Manometry-FTIR data in the standard materials in Fig.

374   5. The data for the glasses appear well correlated (Fig. 5(a)). For the NAMs the samples show a good

375   overall correlation although the water content for PMR-53 appears to be high relative to the other

376   minerals (Fig. 5(b)). The Pakistani olivine shows uniform composition by SIMS as opposed to the

377   significant spread in the FTIR data. An unweighted line-fit has a slope of 1.02, a y-axis intercept of 180

378   ppm H_2O, and r of 0.996 (Fig. 5(a)). The near-unity slope indicates a good correspondence between

379   the methodologies used for analysis as well as consistency with the previously used calibration factors.

380   The high y-axis intercept is notable and is due to the poor fit to the low H_2O NAMs (see Fig. 5(b)). The

381   unweighted regression places effectively equal emphasis on all data and the discrepancy is notable for

382   the low H_2O materials because of the expansion of the scale and the limited range of the data in

383   absolute terms. A better fit is produced by a weighted-line (from Isoplot 3) [41] with weighting based on

384 the measurement uncertainty/dispersion. The weighted line fit has a slope of 1.073 ± 0.058 (95%

385 confidence limit) and an intercept of 6 ± 17 ppm H_2O (95% c.l.), and an MSWD of 5.6. The weighted

386 line fit provides a much better correspondence to the data from the NAMs (Fig. 5(b)).

387

388 The $^{16}O^1H^-$ background of SIMS analysis can be assessed directly through the analysis of the fragment

389 of Suprasil glass that is pressed into the mounts. The $^{16}O^1H^-$ signal emanating from the glass is

390 expected to be dominated by water in the vacuum absorbing on to the target surface. An example of the

391 temporal evolution of ratios of $^{16}O^1H^-/^{30}Si^-$ measured on the Cameca ims-6f from the Suprasil glass in

392 the course of this work are provided in Supplementary file A2/Cameca Dataset 2. Neither SHRIMP

393 $^{16}O^1H^-/^{16}O^-$ nor Cameca $^{16}O^1H^-/^{30}Si^-$ data sets have been corrected for the background measured on

394 the Suprasil glass in order to better evaluate the respective data sets. For the Cameca data, the initial

395 $^{16}O^1H^-/^{30}Si^-$ value for the Suprasil glass is 3.7×10^{-3} and this falls to 6.6×10^{-4} during the analytical

396 session as water is actively pumped from the source chamber. This corresponds to a change in the

397 effective background expressed as water concentration from 37 ppm to 7 ppm for the San Carlos

398 olivine calibration in Table 2. Consistent with the higher source-chamber vacuum pressure in

399 SHRIMP SI, analyses of the Suprasil glass show a range in $^{16}O^1H^-/^{16}O^-$ values from 2 to 4×10^{-5}

400 (approximately 40 to 80 ppm H_2O for the San Carlos olivine grain). The data illustrated in Fig. 6 were

401 obtained in a session with a background $^{16}O^1H^-/^{16}O^-$ of around 2×10^{-5} as measured on Suprasil glass.

402

403 The $^{16}O^1H^-/^{16}O^-$ ratios and the $^{16}O^1H^-/^{30}Si^-$ ratios of each of the glasses and NAM grains from the

404 Cameca ims-6f and SHRIMP SI respectively are presented in Table 2 and illustrated in Fig. 6; analyses

405 from different sessions are given in the supplementary file A2. The glass data are well correlated (Fig.

406 6(a)). An unweighted line fit between the Cameca $^{16}O^1H^-/^{30}Si^-$ and SHRIMP SI $^{16}O^1H^-/^{16}O^-$ has a line

407 of slope 0.000793 and intercept of 3.7×10^{-5} with an r parameter of 0.9996, indicating a near perfect

408 correlation between the two data sets. However, like the Cameca vs the FTIR/manometry data

409 described above, the unweighted line fit has a y-axis intercept that appears high relative to the

410 distribution of the data (Fig. 6(b)). The weighted line fit has a slope of 0.000832 ± 0.000044 (95% conf.

411 limit), with an intercept of $2.8 \pm 0.3 \times 10^{-5}$ and an MSWD of 19. The weighted-line-fit therefore has a

412 lower intercept value than the unweighted-line-fit and produces a better fit to the NAMs data (Fig.

413 6(b)). The MSWD value suggests significant scatter in the data set and this is most apparent in the

414　　NAMs data (Fig. 6(b)), where high precision (and limited dispersion) is coupled with significant scatter

415　　around the best-fit line.

416

417　　These regressions show that there is significant sensitivity of the line-fits to the data sets used. If the

418　　glass data were to be used alone a non-zero intercept would not be surprising given the large

419　　extrapolation towards the y axis. On the other hand, the NAMs data has limited spread and is being

420　　affected by the water background. As noted above, SIMS is a matrix sensitive technique and so

421　　independent calibration of glass and the specific minerals is potentially desirable. However, this yields

422　　calibration lines that are underdetermined in that only two or three samples are used for NAMs, and

423　　even in the glasses there is significant dispersion in several of the samples and the line is dominantly

424　　constrained by the extreme values.

425

426　　If the data are fitted through the analyses of both glass and NAMs, a well-constrained line is

427　　determined (Fig 6(a) and 6(b)). This is perhaps not as surprising as it would seem in that it only

428　　requires relative consistency in sputtering and ionisation of $^{16}O^{1}H^{-}/^{16}O^{-}$ and $^{16}O^{1}H^{-}/^{30}Si^{-}$ of the samples

429　　between SHRIMP SI and the Cameca ims-6f respectively. The good fit in the calibration line simply

430　　indicates that this consistency holds between different SIMS instruments notwithstanding possible

431　　systematic matrix effects affecting the absolute water determination.

432

433　　The internal reproducibility of the SHRIMP analyses appears to be similar to that measured on the

434　　Cameca ims-6f. While the SHRIMP reproducibility for the glasses [expressed as $1\sigma/(^{16}O^{1}H^{-}/^{16}O^{-})*100$

435　　in Table 2] is the highest for ND61 at 1.4%, the variability of $^{16}O^{1}H^{-}/^{30}Si^{-}$ for 36.4 is 5.3%, and the

436　　other glasses have reproducibilities better than 2%. The differences between the means of SHRIMP

437　　data and the means of the Cameca data appear to be consistent within ca. 10 % for the glasses as given

438　　by the deviations from the correlation line (Fig. 6(a)).

439

440　　In comparison, the NAMs measured by SHRIMP SI show greater variability, up to 5%, while the

441　　Cameca data only vary over a range of up to 3%, not including the San Carlos olivine sample that

442　　shows variability at 35%. There appears to be greater dispersion in the analyses than would be

443　　predicted from the internal reproducibility. Nevertheless, excluding the lowest values for Tan-opx and

15

444   San Carlos olivine, the SHRIMP and Cameca data appear to correlate within a range of ca. 20% (Fig.

445   6(b)).

446

447   The main difference between the Cameca ims-6f data and the SHRIMP data is an elevated $^{16}O^1H^-$

448   background in the SHRIMP analyses beyond that expected from measurement of Suprasil glass. A

449   case in point for the SHRIMP data is the comparison of Suprasil glass ($^{16}O^1H^-/^{16}O^- \approx 2 \times 10^{-5}$) and the

450   San Carlos olivine ($^{16}O^1H^-/^{16}O^- \approx 4 \times 10^{-5}$) where both samples should have < 10 ppm water and

451   therefore the measured $^{16}O^1H^-/^{16}O^-$ should be dominated by the contribution from vacuum H_2O.

452   Possible sources of this discrepancy could be related to sample preparation and mount degassing prior

453   to introduction to the SHRIMP vacuum system, or to matrix effects affecting either production of

454    $^{16}O^1H^-$ or $^{16}O^-$ from the glass and olivine targets.

455

456   In order to check the behaviour of these materials after sustained vacuum pumping, two mounts

457   comprising a 25 mm diameter quartz glass disk (Ted Pella, Inc. Product No.16001-2) and a polished

458   metal mount containing San Carlos olivine were placed in the source chamber. After overnight

459   pumping (source chamber pressure reading 9×10^{-9} mbar), the $^{16}O^1H^-/^{16}O^-$ values were consistent with

460   those measured above. After 6 days in the source chamber (pressure reading 7×10^{-9} mbar), the San

461   Carlos olivine had fallen to an $^{16}O^1H^-/^{16}O^-$ of 2×10^{-5} while the quartz glass had remained unchanged

462   at $^{16}O^1H^-/^{16}O^-$ of 2×10^{-5}. As such it appears that the apparent background equilibrated for the two

463   targets after 6 days within the sample chamber. It may be that water sticks to the olivine more

464   aggressively than quartz and some care must be exercised that the olivine has dissipated the surface

465   water prior to analysis. It would also suggest that care should be taken in assessing the level of the

466   background $^{16}O^1H^-/^{16}O^-$ based on Suprasil analyses or San Carlos olivines alone.

467

468   In Figure 7 the SHRIMP $^{16}O^1H^-/^{16}O^-$ data have been background corrected and plotted against the

469   manometry/FTIR data in Table 2. The calibration is performed with a weighted best-fit to all data i.e.

470   glasses, pyroxenes and olivines. The calibration line between SHRIMP $^{16}O^1H^-/^{16}O^-$ and the

471   manometry/FTIR H_2O values has a slope of $1.916 \pm 0.062 \times 10^{-7}$, an intercept of $3.2 \pm 5.3 \times 10^{-6}$ and an

472   MSWD of 14. Given the goodness of the fit, there is little in our data to warrant an individual

473   calibration for the different phases at this stage. Of interest here is the apparently high water content of

474   the San Carlos olivine at ≈80 ppm. If the Suprasil glass is used for background correction, this would

475   still leave a concentration of ≈40 ppm H_2O. But, as noted above, this is a direct artefact of insufficient

476   pump down and vacuum equilibration prior to analysis. However, there is little to suggest the Pakistani

477   olivine has a high background contribution and so the issue with San Carlos olivine may not be a

478   simple mineralogical effect. Moreover, there is no indication in the Tan opx for a residual background

479   effect. At this stage it appears that care will be needed in assessing SHRIMP SI data from NAMs with

480   H_2O concentrations less than 100 ppm. In contrast, the water concentrations in volcanic glasses are

481   well constrained by the combined calibration fit between glasses and NAMs.

482

483   **Discussion**

484

485   **H_2O analyses**

486

487   The excellent agreement between data collected on the SHRIMP SI and data collected on the CIW

488   Cameca ims-6f indicates that both instruments produce ions in a similar way and respond to different

489   matrices in the same way. The main difference between the two data sets pertains to the higher

490   apparent water background in the SHRIMP SI. This is not unexpected given the larger volume of the

491   source chamber and the significantly higher pressure in the SHRIMP SI source chamber.

492

493   The agreement between analyses performed by SHRIMP SI and CIW Cameca ims-6f show that the

494   standard materials are reasonably homogeneous over the surfaces of the materials that have been

495   analysed. In comparison, the manometry-FTIR (M-FTIR) data of Table 2 typically show variability at

496   the 10% level (excluding San Carlos olivine). The discrepancy between M-FTIR and the Cameca H_2O

497   concentrations for the glasses ranges up to 20%, with the largest discrepancy for glass 24.1 (3900 ppm

498   by Cameca/SHRIMP SIMS, 3100 ppm by M-FTIR). This agreement appears to be consistent with

499   previous conclusions that these glasses have water distributed reasonably uniformly throughout. It

500   should again be reinforced that M-FTIR analysis is based on a bulk measurement, whereas SIMS

501   analysis consumes a very small amount of material at a surface. As such, the agreement between the

502   two SIMS techniques is perhaps to be expected as the same samples are effectively being analysed.

503   The correlation between SHRIMP H_2O determinations and the manometry with only a single

504   calibration is quite encouraging.

505

506   Although the measured $^{16}O^1H^-/^{16}O^-$ are consistent during the successive analyses of a single grain,

507   repeated analyses of the same sample but at different times (hours to days apart; within and between

508   different analytical sessions) give varied values for both the Cameca ims-6f and the SHRIMP SI (e.g.,

509   Supplementary file A2). As discussed above, this is likely to be due to a direct artefact of insufficient

510   pump down and vacuum equilibration prior to analysis. Other possible reasons for this variation

511   include localised charging related to the voltage on the electron gun and/or slight changes in the local

512   magnetic field. The different measured $^{16}O^1H^-/^{16}O^-$ ratios from different analytical times can lead to

513   greater errors on the subsequent calibration curves to calculate water contents. The variation on the

514   mineral analyses in the worse case example can lead to approx. 20% error, and therefore the difference

515   between the calibration curves of glass and NAM may lie within this 20% error. These errors can,

516   however, be mitigated by accurately determining the background OH^-. This can be achieved by

517   analysing regularly throughout the session a sample that has little to no water content and subtracting

518   that value from the unknown analyses. Systematic errors to the calibration curve associated with drift

519   (other than background variations) can then be minimised by running standards at the beginning and

520   end of any analytical session and that each mount of unknown samples include at least three standards

521   relevant for the intended study. For example for NAM analyses, one that contains a relatively high

522   water content (e.g., KBH cpx or the Pakistani olivine), one that has a moderate water content (e.g.,

523   Russian Cr-diopside) and one with no or little water (e.g. the anhydrous Suprasil 3002).

524

525   **Matrix Effects**

526

527   Mineral matrix effects are a common phenomenon in ion microprobe analysis and have been apparent

528   almost since the inception of ion microprobe analysis of geological materials. [30,42,43] A matrix effect

529   manifests itself as an ion ratio (atomic or molecular) that differs from the expectation based on

530   concentration differences, or isotope ratio differences, in different mineralogical phases. There appears

531   to be some systematic behaviour in these matrix effects that has been used to try and model the

532   sputtering process, but the more common approach is to use mineral standards that are closely matched

533   in composition to the unknowns to allow empirical correction through fitting of calibration lines.

534

535   As such, we expect to see mineralogical control of the ionisation yields of OH^-, O^- and Si^- used for

536   SIMS calibration. Interestingly, the $^{16}O^1H^-/^{16}O^-$ vs $^{16}O^1H^-/^{30}Si^-$ data from SHRIMP and Cameca are

537   well fitted to a single line. This is not to suggest that there are no matrix effects, but rather the matrix

538   effects between these species are well correlated, and that there is little difference between the

539   sputtering, extraction, and instrumentally induced secondary ion fractionations between the two

540   instruments.

541

542   Of greater importance in our assessment of these standard materials is whether matrix effects between

543   SIMS and FTIR are of consequence. Unfortunately due to the limited dataset of mineral phases, their

544   major element compositions, and water concentrations, it is difficult to conclusively determine whether

545   matrix effects result in significant errors on our mineral calibration line for water concentration. As

546   noted above, a free fit to the data allows the determination of a slope (effectively the calibration

547   coefficient), and an intercept (for the SHRIMP data this is related to the background). For all SHRIMP

548    $^{16}O^1H^-/^{16}O^-$ data and the FTIR glass compositions (wt% H_2O), there is a range from 1.1 to 2.0 x 10^{-7},

549   with intercepts ranging from 3 to 5 x 10^{-5} for the orthopyroxene, clinopyroxene and olivine, up to 3.5 x

550   10^{-4} for the glasses. Thus, while good correlations exist between $^{16}O^1H^-/^{16}O^-$ and wt% H_2O, there is

551   insufficient data to clearly resolve ambiguities in sample water compositions, from any matrix-

552   controlled sputtering behaviour.

553

554   Several FTIR studies have shown that OH^- or H_2O can be incorporated within several sites of the

555   mineral structure. [44,38;] The unknown geometry and charge imbalances associated with the incorporation

556   of water within the mineral structure mean that the OH-bond strengths are also unknown and may be

557   unique to the composition of the mineral. [23,10,11,39] The FTIR absorption coefficients found for a single

558   mineral composition will not be applicable to other minerals of different elemental composition. In

559   addition, differences in OH-bond strengths associated with different mineral compositions mean that

560   there will be differences in the ionisation of the OH^- during analysis on the ion-microprobe, potentially

561   complicating the FTIR ion-probe calibration lines.

562

563 Mosenfelder and Rossman [10,11] recently discussed possible matrix effects of orthopyroxene and

564 clinopyroxene and compared them to analyses of olivine. Mosenfelder and Rossman [10,11] show that any

565 matrix effect is likely to be less than 20%, depending on which absorption coefficient is used for the

566 FTIR water determination. This is close to the level of water variability we see in the samples through

567 variations in all SIMS analysis, and cross referenced to FTIR analysis. At this stage, it would appear

568 that separate standardisation schemes for olivine, orthopyroxene, and clinopyroxene may be

569 unwarranted, and could in fact be detrimental if insufficient numbers of standard materials are

570 available with an appropriate range of water concentration.

571

572 **OH⁻ background limitations**

573

574 The $^{16}O^1H^-$ background measured in SIMS instruments is related to residual H_2O in the vacuum,

575 absorbing onto and desorbing from the sample surface, and specifically the sputter site where surface

576 water can then be sputtered by the Cs^+ primary beam and contribute to the secondary ion beam.

577 Another potential source of the SHRIMP SI OH⁻ background may be related to ionization of OH⁻ at

578 the target by electron impact, induced by the electron beam used for charge compensation arriving at

579 the surface at 1.5 keV. This is similar to the EISIE effect for oxygen ionisation noted in SHRIMP II. [31]

580 However, the OH⁻ production was checked when the Cs gun was turned off and there was no OH⁻

581 emission above detector background.

582

583 In pumping down from atmospheric levels with an unbaked vacuum chamber, water is the main

584 contributor to the residual vacuum at levels down to 10^{-9} mbar. [45] Water is a particularly difficult

585 vacuum residual species because of its propensity to stick to surfaces and hence baking is commonly

586 used to excite water from surfaces. However, regularly taking an ion microprobe source chamber to

587 temperatures in excess of 100 °C can be risky with a complicated set up of components that are not

588 necessarily designed for differential movement induced by thermal expansion.

589

590 Further improvements to the vacuum system that might directly affect $^{16}O^1H^-$ analysis are envisaged

591 for SHRIMP SI. The ion pump on the source chamber was installed to minimise vibration on the

20

592   sample stage. While ion pumps have excellent ultimate vacuum characteristics, they are not the most

593   effective when a gas load is present. The best method for pumping residual water is through a

594   cryogenic pump and we envisage replacing the ion pump with a cryo-pump with appropriate

595   mechanical isolation to minimise vibration. It is expected that this will improve the ultimate vacuum

596   pressure in the source chamber, but will also allow us to get to ultimate background faster after analysis

597   of epoxy mounts.

598

599   The ultimate water background achieved for SHRIMP SI with the ion pump is around 30 ppm (after

600   several days of pumping down in the sample chamber). This background can be quantified and

601   therefore removed by analysing suitable anhydrous materials (such as Suprasil glass) and the correction

602   will be appropriate provided the samples have equilibrated to the vacuum conditions.

603

604   **Reference Materials**

605

606   1. GLASS STANDARDS

607

608   The glasses used here were chosen because they are all of similar major element composition (Table 1)

609   and have water contents determined by FTIR and SIMS ranging from 0.39 to 1.56 wt%. These criteria

610   are essential to create a calibration line that has a slope that is not compromised by a limited range of

611   water contents or significantly different matrix compositions. In addition, because the water content of

612   the most water-rich glass is just below 1.5 wt% compositionally related matrix effects (if any) are

613   limited. [6]

614

615   The structure of the H_2O data from both the Cameca ims-6f and SHRIMP SI are very similar compared

616   to the conventional manometry-FTIR determinations (Fig. 5(a), Fig. 7(a)). Variation of analyses from

617   each glass shard are minimal (<5%) from both the SHRIMP SI and the Cameca 6f showing both that

618   the samples are homogenous to this level and that the reproducibility of both instruments is very good

619   for sub weight percent to weight percent water contents.

620

621   The background extrapolated from the linear correlation in the glass data is quite high suggesting that

622   the SHRIMP analyses have a high background water level of order of 100-200 ppm. However, the

623   intercept of the line-fit is strongly controlled by the lowest analysis (Glass 24.1).   The SHRIMP

624   analysis indicates a higher $^{16}O^1H^-/^{16}O^-$ than the corresponding Cameca $^{16}O^1H^-/^{30}Si^-$ measurement for

625   this glass. As noted above, there is a notable difference between the Cameca water concentration

626   (3900 ppm) and the FTIR determination mean (3100 ppm). It is likely that this glass might be slightly

627   more heterogeneous than other glasses and its use on the calibration line may create excess variability

628   where it can cause a significant change in the intercept of the calibration line. The calibration is lacking

629   a suitable glass with very low water content to better constrain the line fit if only glasses are to be used.

630

631   Caulfield et al. [16] used the CIW Cameca 6f SIMS and the ANU FTIR instrument to analyse water

632   within the glass shards used to aid their U-Th-Ra model of fluid-flux melting at the Fonualei Spreading

633   Center and Valu Fa Ridge, Tonga. Similar to our findings here, they found that there was a good

634   agreement between the FTIR and SIMS determined water concentrations. [16] However, FTIR and

635   Cameca ims-6f determined water contents of ND61 and ND69 presented in Table 2 are 12-15 wt%

636   higher than those found by both the Caulfield et al. [16] study, as well as those presented in Lloyd et al. [17]

637   The multiple analyses of individual glass shards by various instruments indicate that individual glass

638   shards are homogenous (Table 2). Therefore, the discrepancy between the water contents found in the

639   glass samples from our study compared to both Caulfield et al. [16] Lloyd et al. [17] reflects true differences

640   in water concentrations between glass shards from the large sample batch.

641

642   2. NOMINALLY ANHYDROUS MINERALS

643

644   Major element compositions for many of the nominally anhydrous minerals are similar to those in

645   previously published studies on these minerals (PMR-53 cpx, KBH-opx [13]; KBH-cpx [1]; Rus Cr-diop

646   [19,20]; Tan-opx [25]). The exception being the Pakistani olivine sample that has approximately 4 wt% more

647   MgO and FeO^t (Table 1) than the grain analyses in the Gose et al. [22] study. These differences are likely

648   to result from variations in the amount of serpentinsation of individual olivine grains within individual

649   veins of the dunitic rock.

650

651   The background vacuum water contribution to SHRIMP SI $^{16}O^1H^-/^{16}O^-$ determinations is clearly an

652   issue for samples with less than 100 ppm H_2O. For SHRIMP SI calibrations below this concentration

653   level, a secondary standard such as San Carlos olivine will allow confirmation that the samples have

654   equilibrated in the vacuum system and that Suprasil glass allows an appropriate background correction.

655

656   Mineral matrix effects in ion-probe analysis, associated with differences in intra and interphase

657   compositions, is likely to be an important control in the mineral specific water calibration lines.

658   However at this stage the perturbations caused by matrix effects are possibly at a similar level to the

659   heterogeneity in the samples used for calibration. Mosenfelder and Rossman [10,11] recently discussed

660   the possible matrix effects of orthopyroxene and clinopyroxene and compared them to the analyses of

661   olivine. Mosenfelder and Rossman [10,11] show that matrix effect is less than 20%, depending on which

662   absorption coefficient is used for the FTIR water determination. This is of a similar magnitude to the

663   dispersion around the best-fit lines for SIMS data versus manometry-FTIR (Fig. 5, 7). With a limited

664   number of standard materials, finding systematic differences in terms of apparent water content that

665   can be interpreted as matrix effects as opposed to real variation in the targets is difficult.

666

667   3. POSSIBLE NAM STANDARDS FOR WATER DETERMINATION BY FTIR AND SIMS

668   .

669   To acquire calibration lines for analysing water in NAMs by the SHRIMP SI (or any SIMS instrument)

670   a set of mineral standards with a range of 10-500 ppm water concentrations must be characterized, and

671   be homogenous in regards to water concentrations. We have therefore concentrated on analysing

672   minerals that have H_2O measurements from vacuum extraction manometry (e.g. KBH-1 opx, PMR-53

673   cpx) [13] and have also begun to look at pyroxene and olivine inclusion free gemstones that have the

674   potential to be future standards for water analyses.

675

676   Pakistani olivine has a hydrothermal origin, and therefore there are some grains that contain inclusions

677   that will need to be avoided if it is to be used as a standard. [22,23,24] Additionally, there is a huge grain-to-

678   grain variation in water contents. In this study we examined an exceptionally water-rich sample that

679   has about 340 ppm H_2O, whereas the sample investigated by Kovács *et al.* [23] only contained 72 ppm

680   H_2O. It is thus essential that each Pakistani Olivine grain used for SIMS measurements is first analysed

681   by FTIR and water contents should be quantified using the absorption coefficient of 0.57 ± 0.04 from

682   Kovács *et al.* [23]

683

684   PMR-53 cpx, KBH cpx and KBH-1 opx are currently being used (along with ROM-XXX samples from

685   the study of Bell *et al.* [46]) as pyroxene standards by several SIMS and FTIR laboratories worldwide.

686   While there can be considerable differences in the OH^- from different sessions and different

687   instruments, consistent correlations of these samples from each analytical session suggest that there is

688   no significant heterogeneity among the different standards used by the different laboratories. Therefore

689   PMR-53 cpx, KBH cpx and KBH-1 opx should be used for SIMS and FTIR standards for water

690   determinations of pyroxene. Mosenfelder and Rossman, [11] however, do point out that standard PMR-53

691   cpx is a 'problem sample' because it plots at too low H content and/or too high SIMS $^{16}O^1H^-/^{30}Si^-$

692   ratios compared to the other clinopyroxene samples (e.g. Fig. 5). While this observation is disturbing,

693   because the PMR-53 cpx has been studied by multiple techniques and was used by Bell et al. [13] to

694   determine the FTIR absorption coefficients for clinopyroxene, there is no satisfactory answer to why it

695   plots so far off SIMS calibration lines [11] and until this issue is resolved, we suggest PMR-53 cpx is not

696   used as a standard for FTIR or SIMS clinopyroxene water studies.

697

698   Aubaud *et al.* [26] indicate that their studied grain of San Carlos olivine has water contents generally less

699   than 1 ppm. We have investigated a large number (> 25) of mm-sized San Carlos olivine cubes with IR

700   spectroscopy and most samples have water contents at or below the detection limit of about 1 ppm.

701   However, the FTIR analysis of the San Carlos olivine-2 grain presented here shows that some grains

702   can have approximately 10 ppm H_2O (Fig. 3, Table 3). Also Li *et al.* [27] reported San Carlos olivine

703   with 2-4 ppm H_2O. Similar findings have been found for some major and trace elements within

704   different sized grains of San Carlos olivine. [47] The heterogeneity of OH^- between different San Carlos

705   olivine grains of different sizes suggests that it too should only be used as a reliable standard for low

706   water concentrations if it is first characterised by FTIR measurements.

707

708   The Russian Cr-diopside and Tanzanian orthopyroxene also appear to have minimal variation in

709   respect to major element and water concentrations within single grains during a single analytical

710   session (Supplementary file A2). This agrees well with recent FTIR studies of Moesenfelder and

711   Rossman [10,11] and we conclude that these two readily available gemstones, that are generally free of

712   inclusions and contain homogenous water contents, might be suitable as standards for water analyses.

713   If the water contents of these minerals can be determined independently by an absolute method (i.e.,

714   manometry), these NAMs are therefore ideal candidates for international laboratory standards.

715

716   **Conclusions**

717

718   The SHRIMP SI has been used to measure water concentrations for the first time in a series of

719   reference materials. The data have been compared with measurements of the same mounts on the

720   Cameca ims-6f at CIW, and with FTIR measurements on fragments of the same materials at ANU.

721   SHRIMP SI analysis of NAMs with less than 100 ppm water is somewhat problematical because of the

722   water background contributed by the vacuum (≈30 ppm), and the variable retention of water on the

723   surfaces of mineral grains. The background can be monitored by analyses of Suprasil glass in

724   conjunction with San Carlos olivine as a secondary near water-free standard. Despite the background

725   issues for NAMs, the SHRIMP data are well correlated to Cameca ims-6f data and FTIR data and

726   SHRIMP SI appears capable of determining water concentrations in volcanic glasses at 500 to 15,000

727   ppm levels in its current configuration.

728

729   A set of natural and/or synthetic NAMs standards need to be developed and used as inter-laboratory

730   standards for both FTIR and ion-probe studies. These standards need to be both homogenous in

731   composition and water contents. Ideally, during each SIMS analytical session three matrix-matched

732   standards (one blank, and two variable water contents) should be run periodically. The samples used by

733   Bell *et al*. [13] and Rossman and Bell [1] along with the samples of Bell *et al*. [46] (not studied here) should be

734   used as inter-laboratory standards for water analyses of NAM. In addition once the absolute water

735   concentration of the Russian Cr-diopside and the Tanzanian orthopyroxene are made, then these

736   samples could also be used as FTIR and SIMS NAM standards for water determination.

737

750

751

752   **Notes and References**:

753

754   [a]Department of Earth and Planetary Sciences, Macquarie University, NSW, Australia

755   [b]Research School of Earth Sciences, Australian National University, ACT, Australia

756   [c]Géosciences Montpellier, University of Montpellier & CNRS, Place E. Bataillon 34095 Montpellier

757   cedex 5, France

758   [d]Carnegie Institution of Washington, 5424 Broad Branch Road, Washington, D.C. 20005, USA

759

760   1.   D.R. Bell, G.R. Rossman, *Science*, 1992, **255**, 1391-1397.

761   2.   E. Stolper, S. Newman, *Earth Planet. Sci. Lett.,* 1994, **121**, 293–325.

762   3.   A.V. Sobolev, M. Chaussidon, *Earth Planet. Sci. Lett.,* 1996, **137**, 45–55.

763   4.   J. Blundy, K.V. Cashman, *Geology,* 2005, **33**, 793–796.

764   5.   T. Plank, K.A. Kelley, M.M. Zimmer E.H. Hauri, P.J. Wallace, *Earth Planet. Sci. Lett.,*. 2013,

765   **364**, 168-179.

766   6.   E.H. Hauri, J. Wang, J.E. Dixon, P.L. King, C. Mandeville, S. Newman, *Chem. Geol.,* 2002,

767   **183**, 99–114.

768   7.   K. Koga, E.H. Hauri, M.M. Hirschmann, D.R. Bell, *Geochem. Geophys. Geosys.,* 2003, **4.2**

769   1019. Doi:10.1029/2002GC000378.

770   8.   E.H. Hauri, G.A. Gaetani, T.H. Green, *Earth Planet. Sci. Lett.,* 2006, **248**, 715-734 doi:

771   10.1016/j.epsl.2006.06.014.

772   9.   J. Wade, T. Plank, .M. Zimmer, E.H. Hauri, K. Roggensack, K. Kelley, *Geology,* 2008, **36**,

773   799–802.

774   10.   J.L. Mosenfelder G.R. Rossman, *Am. Mineral.,* 2013a, **98**, 026-1041

775   doi:10.2138/am.2013.4291

776   11.   J.L. Mosenfelder G.R. Rossman, *Am. Mineral.,* 2013b, **98**, 1042-1054

777   doi:10.2138/am.2013.4413

778   12.   E. Libolwitzky, G.R. Rossman, *Phys. Chem. Minerals.,* 1996, **23**, 319-327.

779   13.   D.R. Bell, P.D. Ihinger, G.R. Rossman, *Am. Mineral,,* 1995, **80**, 465–474.

780   14.   N.S. Keller, R.J. Arculus, J. Hermann, S. Richards, *J. Geophys. Res. Solid Earth,* 2008, **113**

781   B08S07.

782   15.   J.M. Sinton, L.L. Ford, B. Chappell, M.T. McCulloch, *J. Petrol.,* 2003, **44**, 159-195.

783   16.   J. Caulfield, S. Turner, R. Arculus, C. Dale, F. Jenner, J. Pearce, C. Macpherson, H. Handley,

784   *J. Geophys Res.,* 2012, **177**, B11209 doi:10.1029/2012JB009526.

785   17.   A.S. Lloyd, T. Plank, P. Ruprecht, E.H. Hauri, W. Rose, *Contrib. Mineral. Petrol.,* 2013, **165**,

786   129–153.

787   18.   R.D. Shannon, J.E. Dickinson, G.R. Rossman, *Phys. Chem. Minerals,* 1992, **19**, 148-156.

788   19.   J. Ingrin, N. Doukhan, J.C. Doukhan, *J. Geophys. Res. Solid Earth,* 1991, **96(B9)**, 14287-

789   14297 doi:10.1029/91JB01233

790   20.   J. Ingrin, S. Hercule, T. Charton, *J. Geophys. Res. Solid Earth,* 1995, **100(B8)**, 15489-15499

791   doi:10.1029/95jb00754

792   21.   J. Gose, P. Reichart, G. Dollinger E. Schmädicke, *Am. Mineral.* 2008, **93**, 1613-1619.

793   22.   J. Gose, E. Schmädicke, M. Markowitz, A. Beran, *Mineral. Petrol.,* 2010, **99**, 105-111.

794   23.   J. Kovacs H. O'Neill J. Hermann E.H. Hauri *Am. Mineral.,* 2010, **95**, 292-299

795   doi:10.2138/am.2010.3313

796   24.   P. Boulhol, J.P. Burg, J.L. Bodinier, M.W. Schmidt, S.M. Bernasconi, H. Dawood, *Can.*

797   *Mineral.,* 2012, **50**, 1291-1304.

798   25.   A. Beran, J. Zemann, *Tschermaks Mineralogische and Petrographische Mitteilungen* 1986, **35**,

799   19-25.

800 26. C. Aubaud, A.C. Withers, M.M. Hirschmann, Y. Guan, L.A. Leshin, S.J. Mackwell, D.R. Bell,
801 *Am. Mineral.,* 2007, **92**, 811-828.

802 27. Z-X.A. Li C-T.A. Lee A.H. Peslier A. Lenardic S.J. Mackwell *J. Geophys. Res. Solid Earth,*
803 2008, **113(B9),** B09210 doi:10.1029/2007jb005540

804 28. T.R. Ireland, S. Clement, W. Compston, J.J. Foster, P. Holden, B. Jenkins, P. Lanc, N. Schram,
805 I.S. Williams, *Australian J. Earth Sci.,* 2008, **55**, 937-954.

806 29. H. Matsuda, *Int. J. Mass Spectrom. Ion Phys.,* 1974, **14**, 219-233.

807 30. T.R. Ireland, N. Schram, P. Holden, P. Lanc, J. Avila, R. Armstrong, Y. Amelin, A. Latimore,
808 D. Corrigan, S. Clement, J.J. Foster, W. Compston, *Int. J. Mass Spectrometry* 2014, **359**, 26-
809 37.

810 31. R.B. Ickert, J. Hiess, I.S. Williams, P. Holden, T.R. Ireland, P. Lanc, N. Schram, J.
811 Foster, S.W. Clement *Chem. Geol.* 2008, **257**, 114-128.

812 32. T.R. Ireland, *Geochim. Cosmochim. Acta*, 1988, **52,** 2827-2839.

813 33. A.J. Fahey, J.N. Goswami, K.D. McKeegan, E. Zinner, *Geochim. Cosmochim. Acta,*1987, **51**,
814 329-350.

815 34. J.E. Dixon, E.M. Stopler, J.R. Halloway, *J. Petrol.,* 1995, **36**, 1607-1631.

816 35. P.D. Ihinger, R.L. Hervig, P.F. McMillan, *Reviews in Mineralogy,* 1994, **30,** 67-121.

817 36. E. Stopler, *Geochimica et Cosmochimica Acta,* 1982, **46**, 2609-2620.

818 37. C.W. Mandeville, J.D. Webster, M.J. Rutherford, B.E. Taylor, A. Timbal, K. Faure, *Am.*
819 *Mineral.* 2002, **87**, 813-821

820 38. A.J. Berry, H. O'Neill, J. Hermann, D.R. *Scott, Earth. Planet. Sci. Lett.,* 2007, **261**, 134-142.

821 39. J. Ingrin, I. Kovacs, E. Deloule, E. Balan, M. Blanchard, S.C. Kohn, J. Herman, *Am. Mineral.,*
822 2014, **99**, 2138-2142.

823 40. D.R. Bell, G.R. Rossman, J. Maldener, D. Endisch, F. Rauch, *J. Geophys. Res. Solid Earth,*
824 2003 **108(B2)** doi:2105 Artn 2105.

825 41. K. Ludwig, *Berkeley Geochronology Center Special Publication* 2012 *5*,.

826 42. N. Shimizu, S.R. Hart, *Annual Review of Earth and Planetary Sciences*, 1982 **10,** 483.

827 43. T.R. Ireland, in: *Hyman, M., Rowe, M. (Eds.), Advances in Analytical Geochemistry.* JAI Press,
828 Greenwich 1995, 1-118.

829 44. E. Libolwitzky, A.Beran, *Phys. Chem. Mineral.* 1995, **22**, 387-392.

830   45.   D. Hoffman, B. Singh, J.H. Thomas III *Handbook of Vacuum Science and Technology,* 1998,

831   835 pp.

832   46.   D.R. Bell, G.R. Rossman, R.O. Moore, *J. Petrol.,* 2004, **45**, 1539-1564

833   47.   J.H. Fournelle, *Microsc. Microanal.,* 2011, **17**, S2, 842-843.

834

835

836   **Figure captions**

837

838   **Fig. 1.** Schematic illustration of the SHRIMP SI at The Australian National University, Canberra,

839   Australia.

840

841   **Fig. 2.** ^{17}O and $^{16}O^{1}H$ peak resolution of the SHRIMP SI. (a) Linear scale for counts per second and (b)

842   log scale.

843

844   **Fig. 3.** FTIR absorption peaks of basaltic glasses used in this study, normalised to 1 cm sample

845   thickness.

846

847   **Fig. 4.** Uncorrected FTIR absorption spectra for olivines and pyroxenes measured in this study.

848   Baselines are shown with dashed lines (raw and corrected data can be found in the SupplementaryData
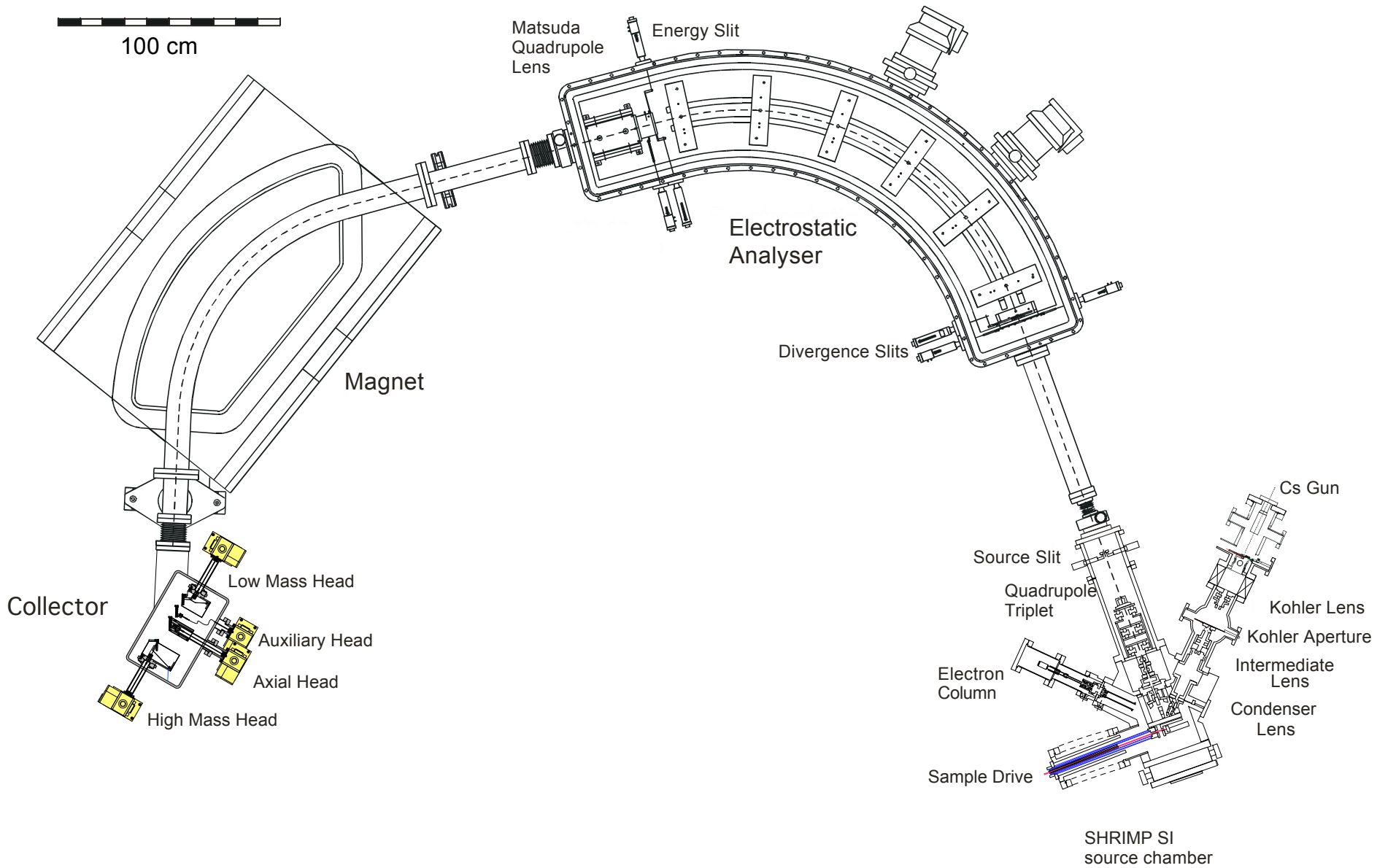
849   A1).

850

851   **Fig. 5.** OH^{-} measurements from the Cameca ims-6f ($^{16}O^{1}H^{-}/^{30}Si^{-}$) compared to those obtained from

852   manometry and FTIR for basaltic glasses and NAMs. Error bars represent the spread in the data. (a)

853   scale to show all glass and NAMs data, (b) scale to highlight NAMs data. Best-fit lines are plotted for

854   an unweighted regression (thicker broken line), and a weighted-line fit (solid line with thinner broken

855   lines as the 95% confidence limit of the data). Weighted line fit from IsoPlot 3 (Ludwig [41]). The

856   unweighted line is not well fitted to the NAMs data but a weighted line fit is appropriate for the whole

857   data set with the correlation passing close to the origin and all data within ≈10% of the weighted line fit.

858   SCO = San Carlos olivine.

859

860 **Fig. 6.** OH⁻ measurements from the SHRIMP SI ($^{16}O^1H^-/^{16}O^-$) compared to those obtained from the

861 Cameca ims-6f ($^{16}O^1H^-/^{30}Si^-$) for glasses and NAMs. (a) Scale to show all glass and NAMs data, (b)

862 scale to highlight NAMs data. Best-fit lines are plotted for an unweighted regression (thicker broken

863 line), and a weighted-line fit (solid line with thinner broken lines as the 95% confidence limit of the

864 data). Weighted line fit from IsoPlot 3 (Ludwig [41]). SCO = San Carlos olivine. The SHRIMP $^{16}O^1H^-$

865 $/^{16}O^-$ data are well correlated with the Cameca $^{16}O^1H^-/^{30}Si^-$ and a satisfactory weighted line fit is

866 apparent. However, the SHRIMP data have an apparent background $^{16}O^1H^-/^{16}O^-$ level of $\approx$3 x 10⁻⁵

867 which is due to the higher vacuum pressure in the SHRIMP SI source chamber compared to the

868 Cameca ims-6f chamber. At these pressure levels, the main species in the vacuum is water. San

869 Carlos olivine (SCO) is distinctly high in this data set; on extended pumping the $^{16}O^1H^-/^{16}O^-$

870 background can be improved to a level $\leq$2x10⁻⁵, similar to the value for Suprasil glass.

871

872 **Fig. 7**. SHRIMP SI H_2O concentrations in glasses and NAMs determined after background correction

873 and calibration to FTIR or vacuum extraction manometry measurements. The calibration is based on

874 the weighted line fit to all data.   (a) Scaled to show all glass and NAMs data, (b) scaled to highlight

875 NAMs data.

876

100 cm

Matsuda
Quadrupole
Lens

Energy Slit

Electrostatic
Analyser

Magnet

Divergence Slits

Collector

Low Mass Head

Auxiliary Head

Axial Head

High Mass Head

Cs Gun

Source Slit

Quadrupole
Triplet

Kohler Lens

Kohler Aperture

Intermediate
Lens
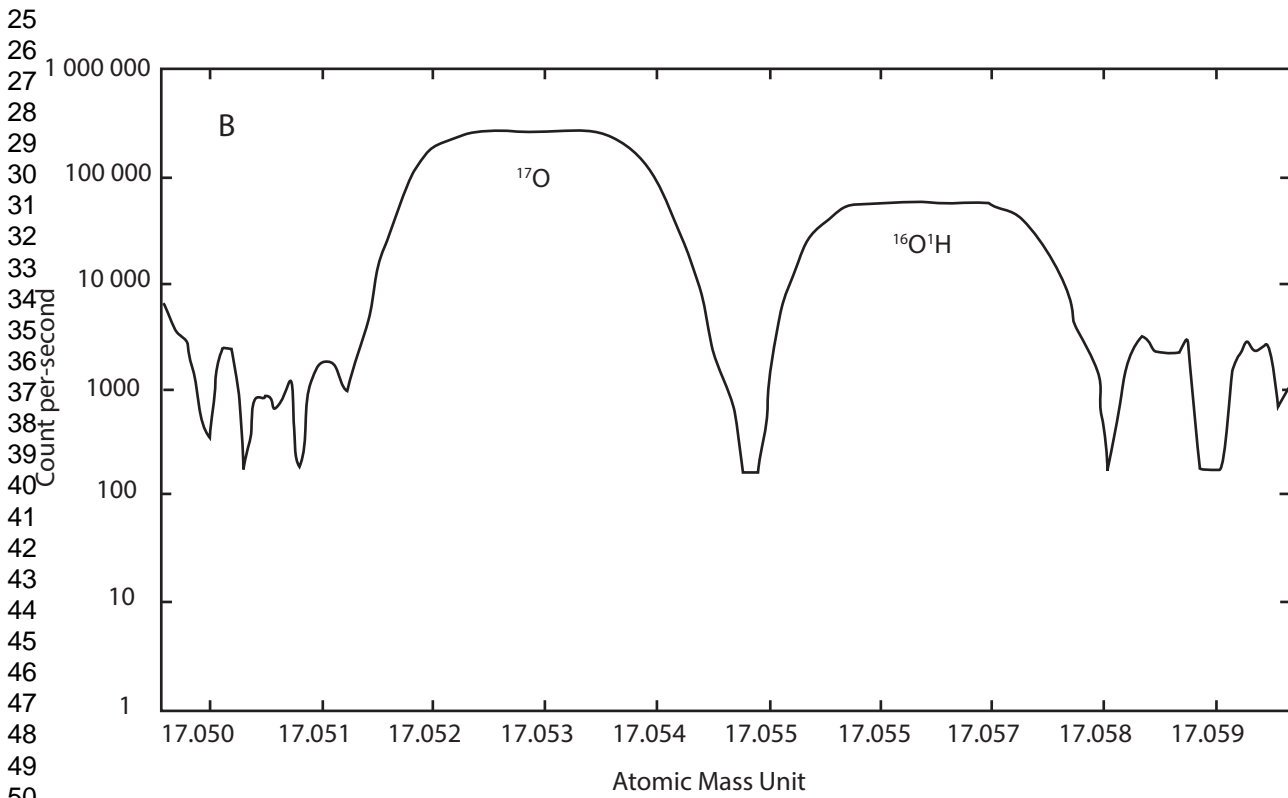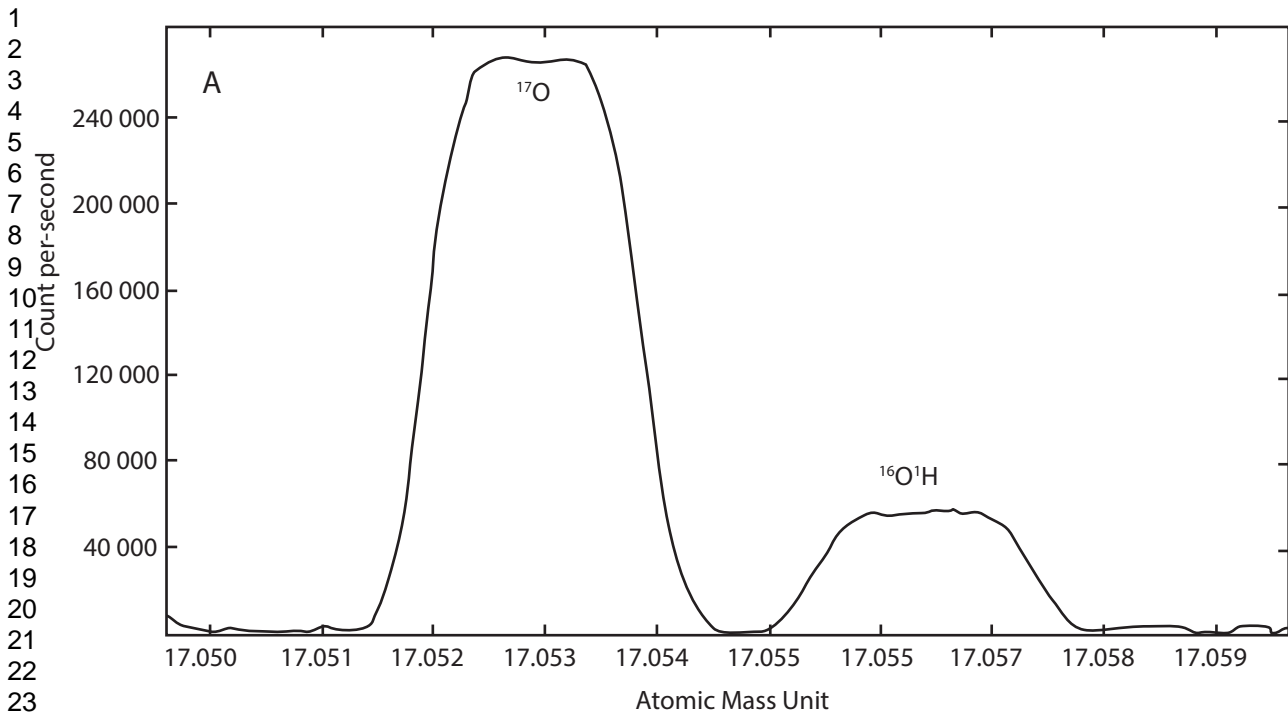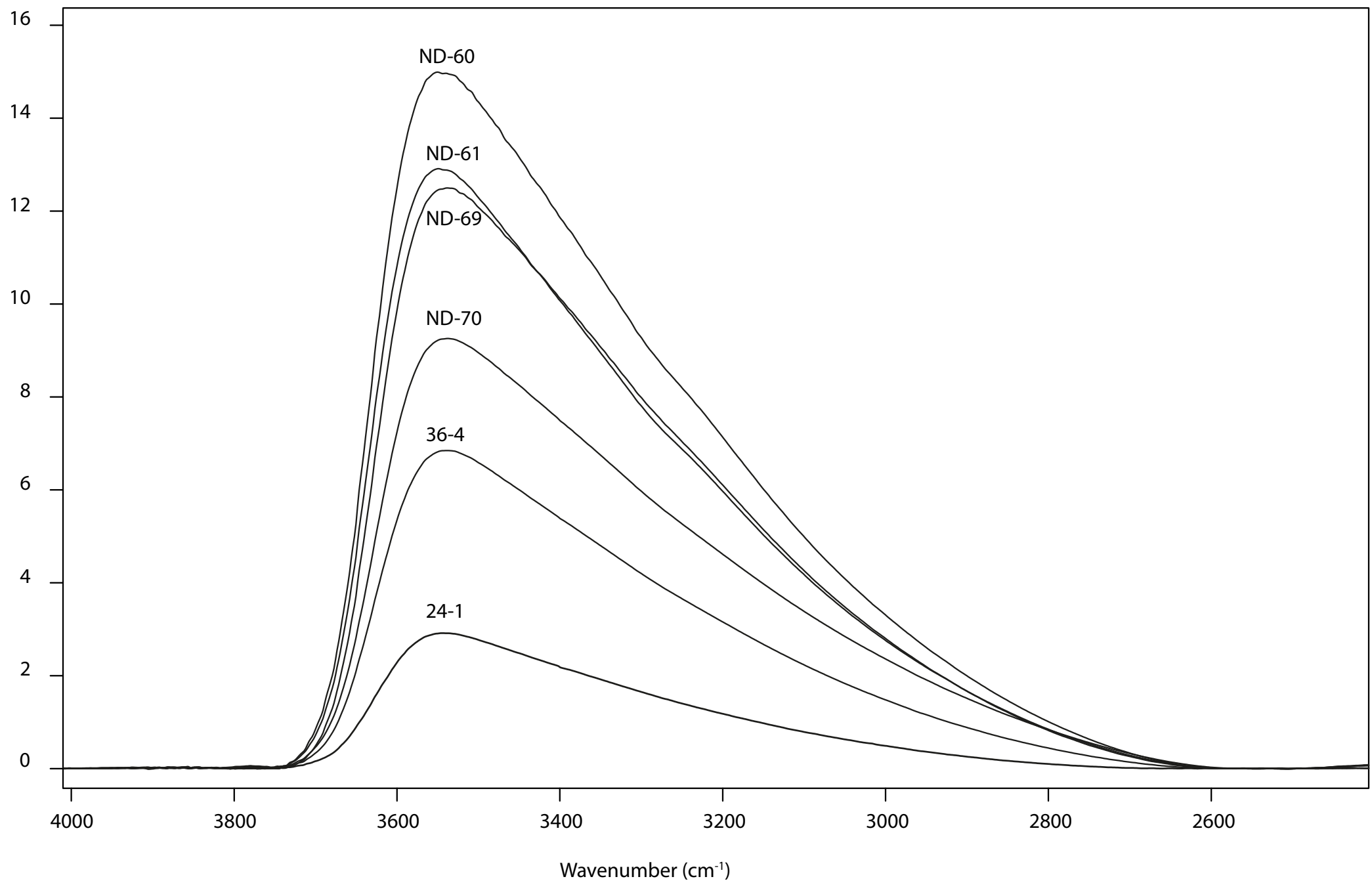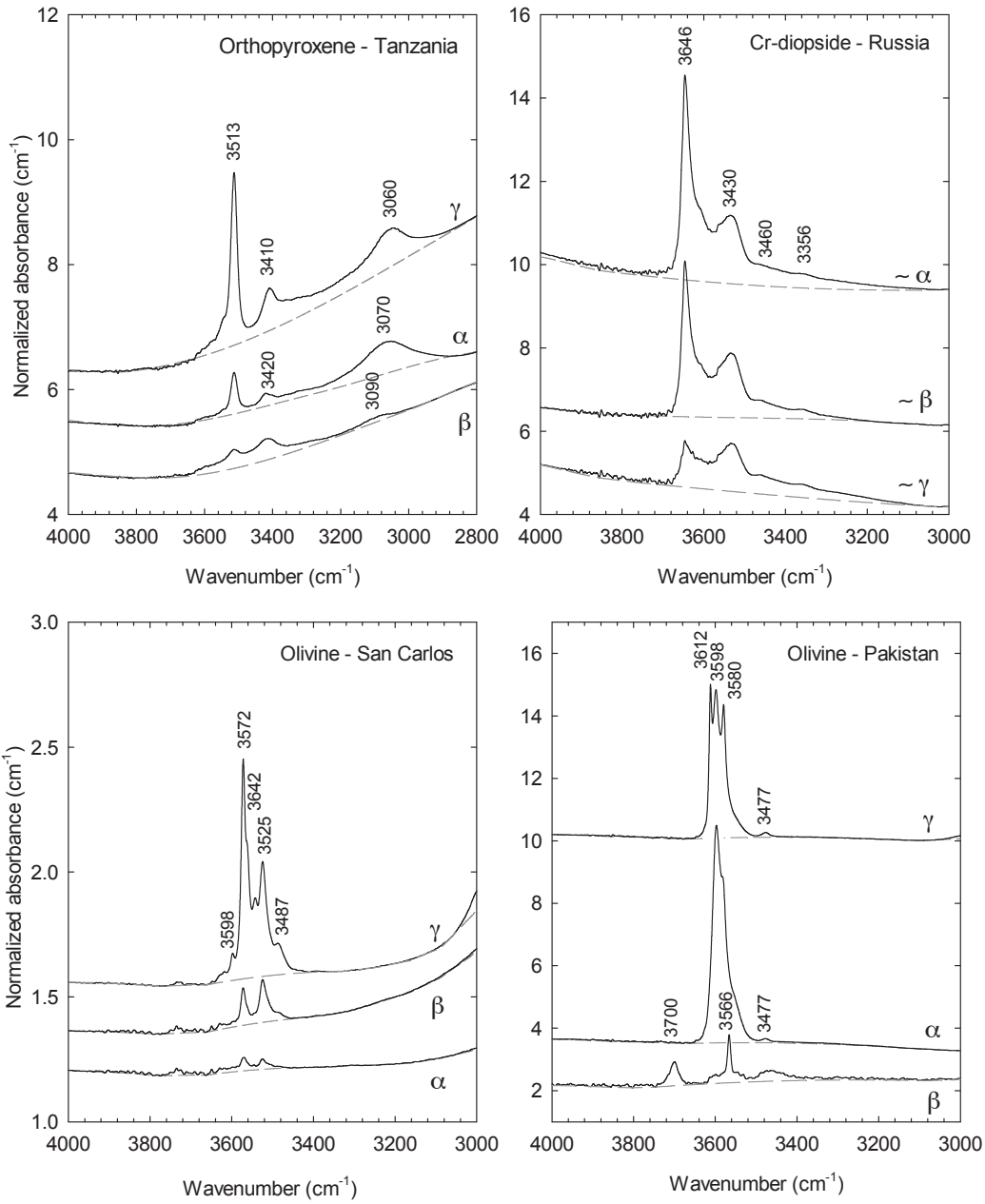
Electron
Column

Condenser
Lens

Sample Drive

SHRIMP SI
source chamber

Figure 3

Figure 4

1
2
3
4
5
6
7
8
9
10
11
12
13
14
15
16
17
18
19
20
21
22
23
24
25
26
27
28
29
30
31
32
33
34
35
36
37
38
39
40
41
42
43
44
45
46
47
48
49
50
51
52
53
54
55
56
57
58
59
60

Figure 5(a)

Figure 5(b)

1
2
3
4
5
6
7
8
9
10
11
12
13
14
15
16
17
18
19
20
21
22
23
24
25
26
27
28
29
30
31
32
33
34
35
36
37
38
39
40
41
42
43
44
45
46
47
48
49
50
51
52
53
54
55
56
57
58
59
60

Figure 6(a)

Figure 6b

Figure 7a

1
2
3
4
5
6
7
8
9
10
11
12
13
14
15
16
17
18
19
20
21
22
23
24
25
26
27
28
29
30
31
32
33
34
35
36
37
38
39
40
41
42
43
44
45
46
47
48
49
50
51
52
53
54
55
56
57
58
59
60

Figure 7b

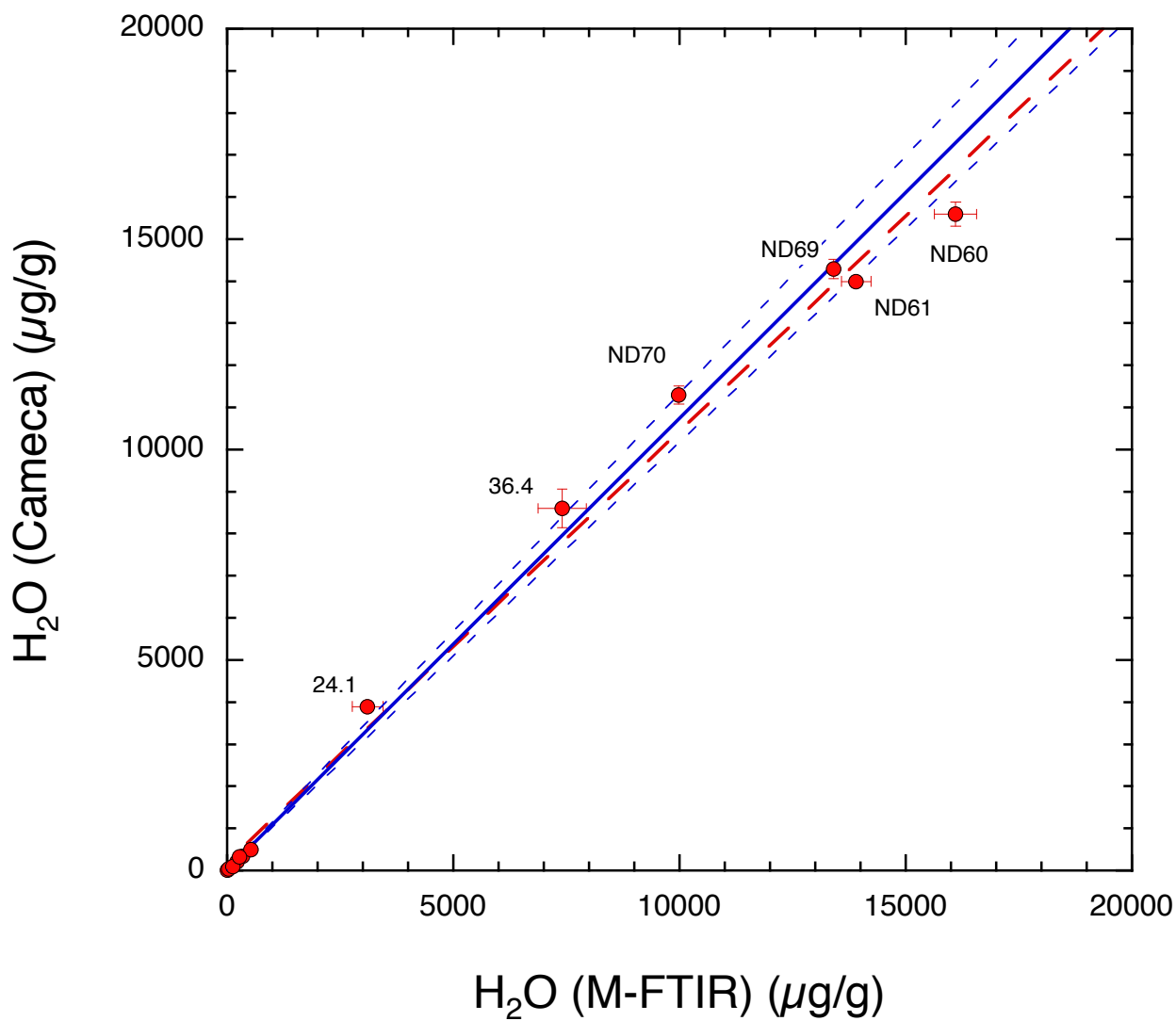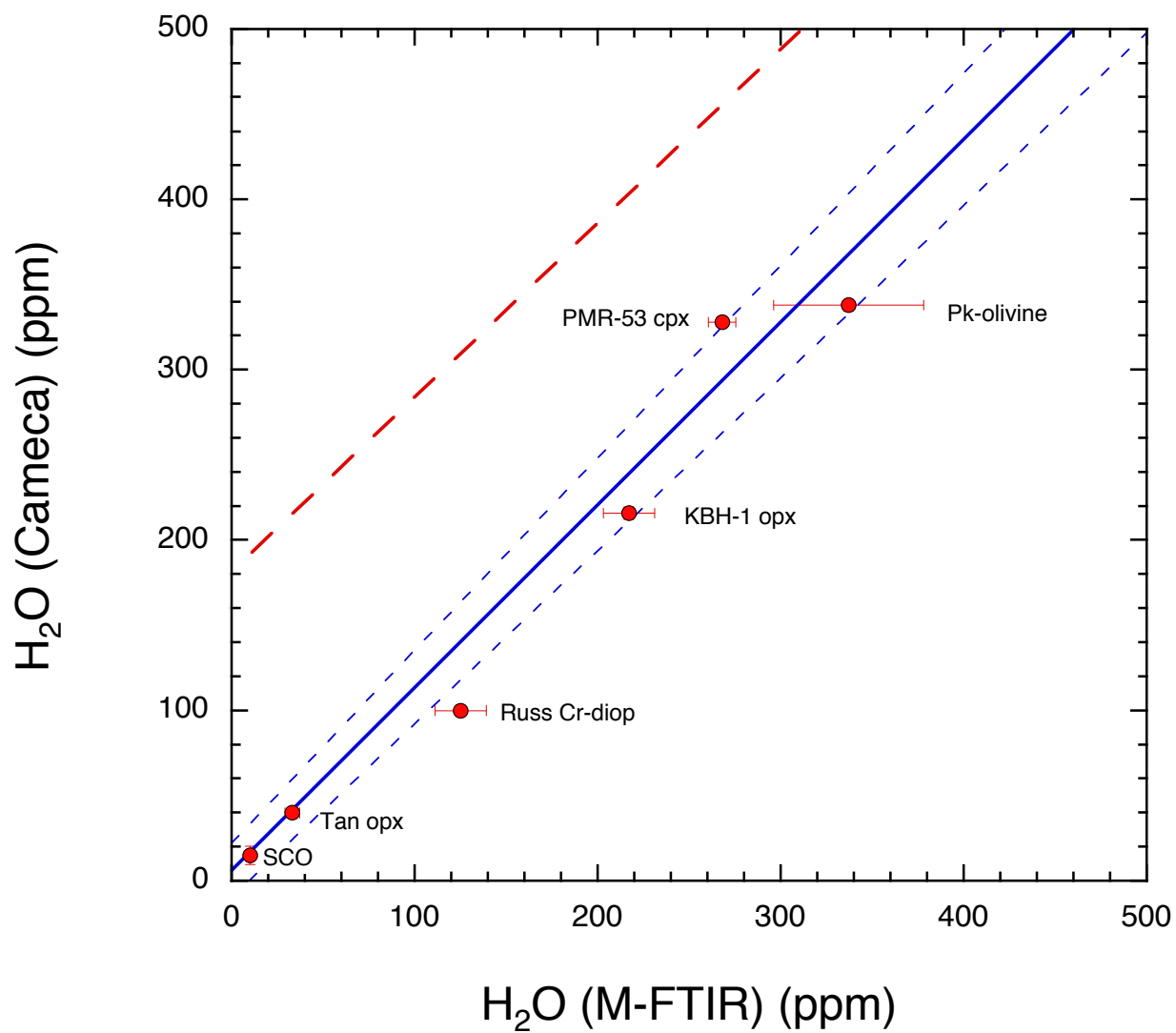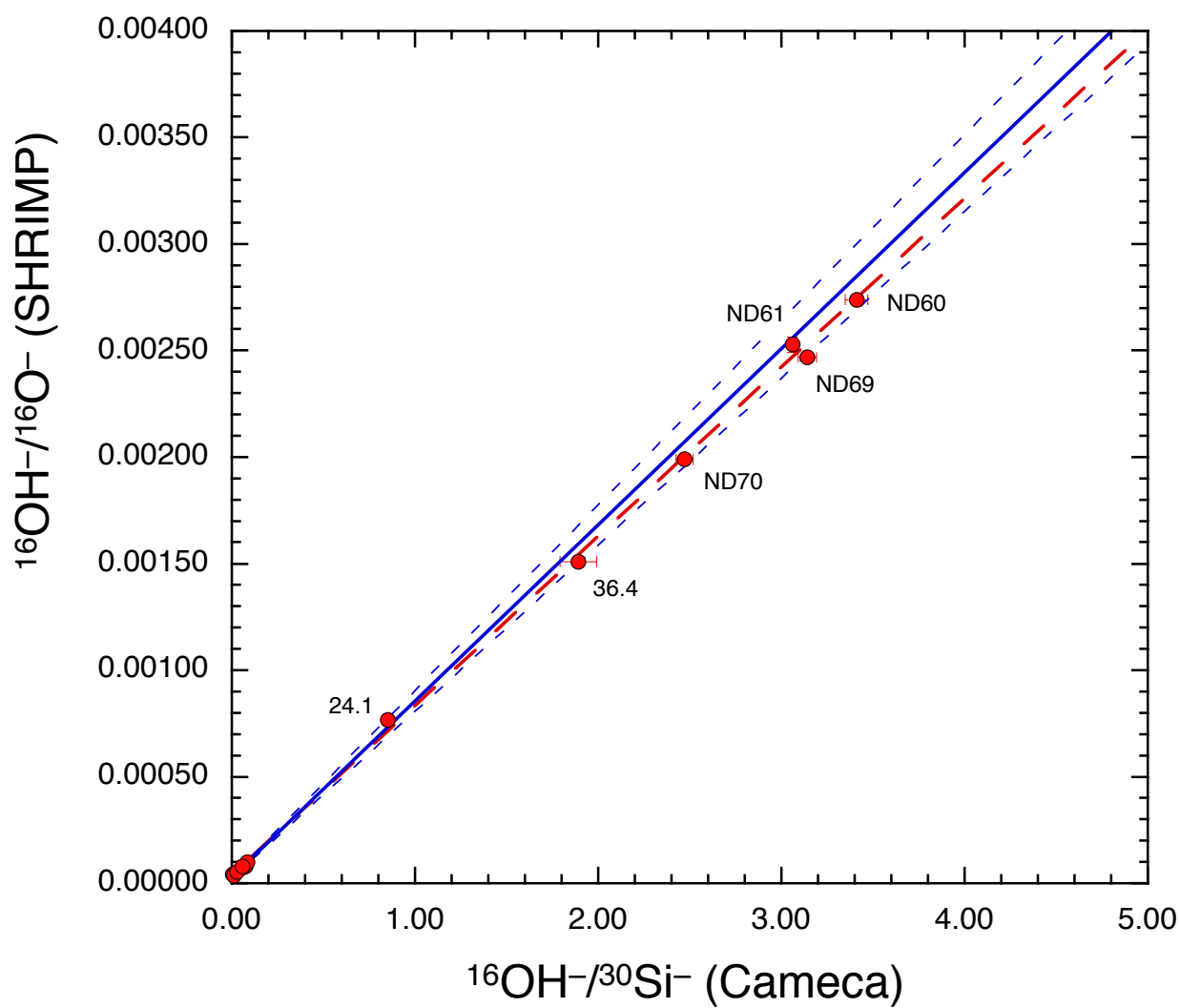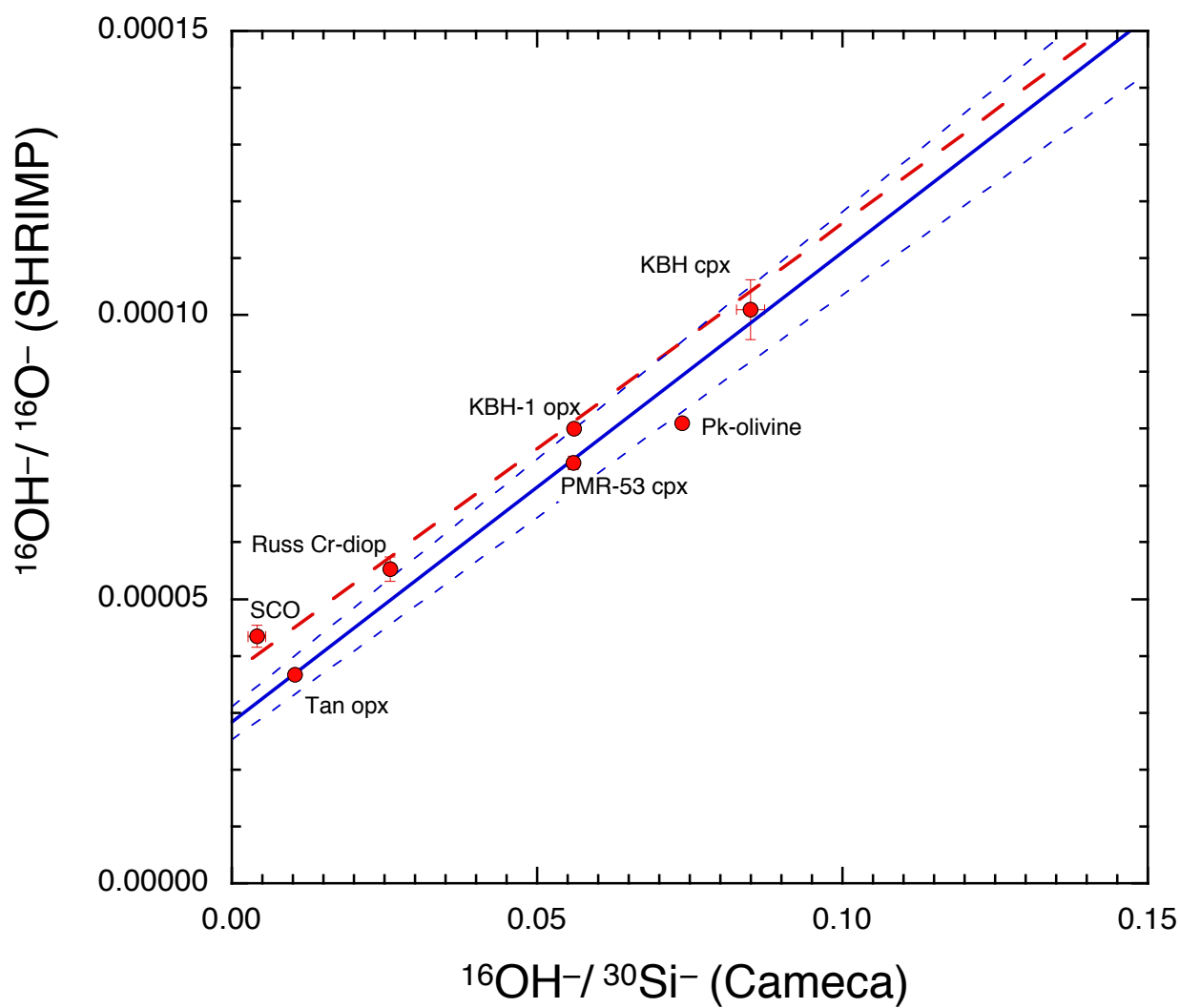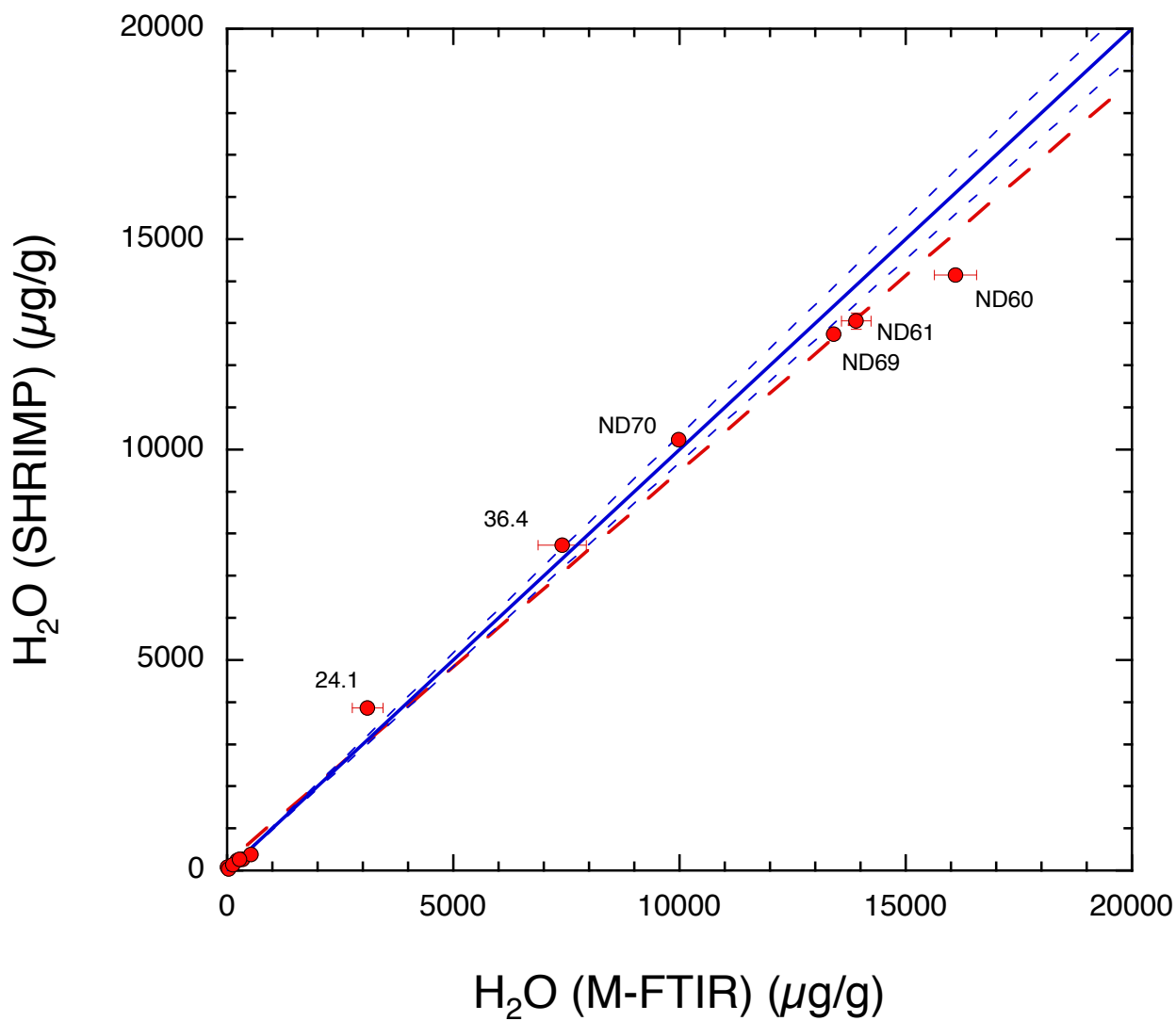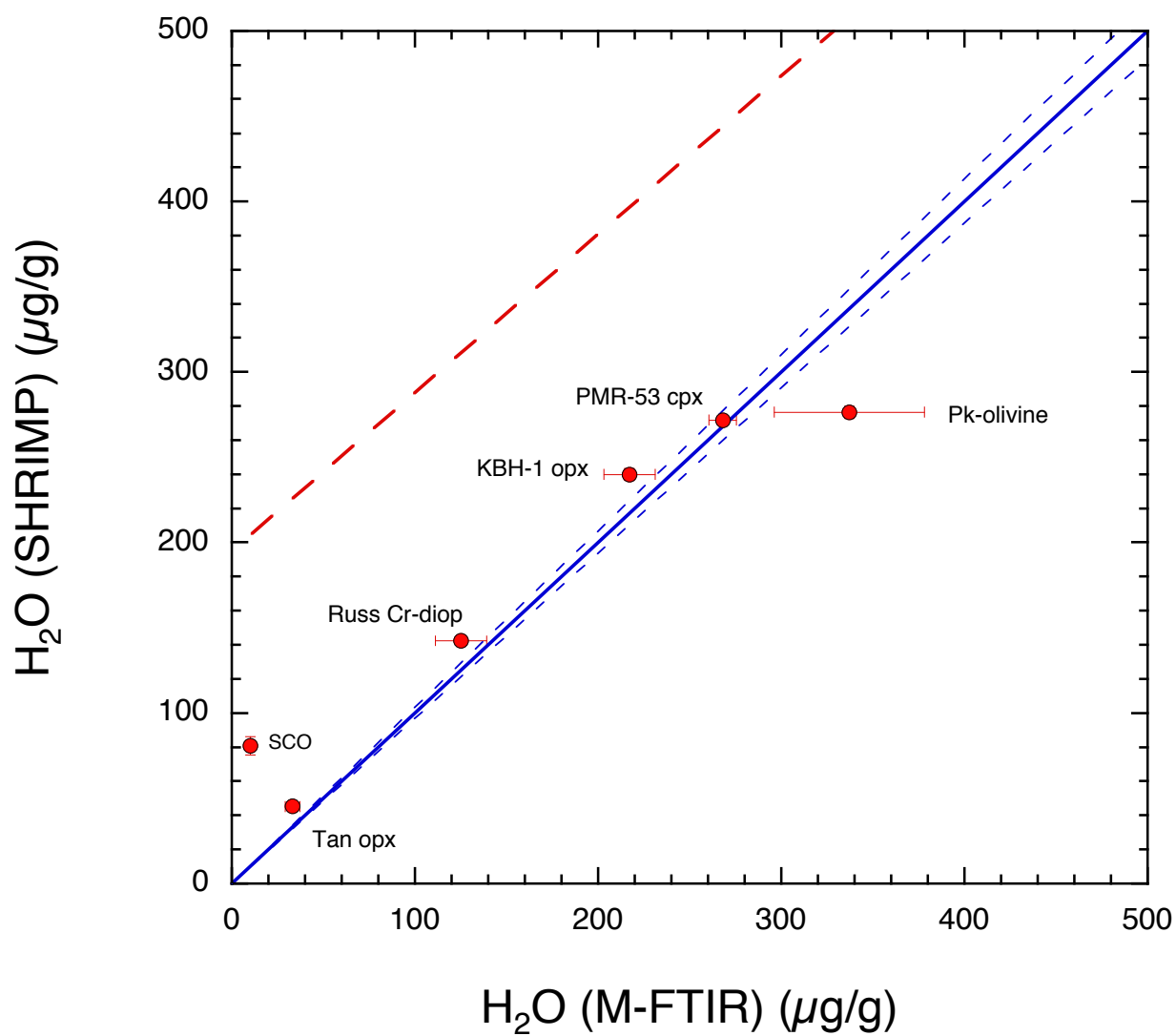Table 1: Electron microprobe analyses of glass and mineral samples

	SiO$_2$	TiO$_2$	Al$_2$O$_3$	Cr$_2$O$_3$	FeO^t	MnO
Glass						
36.4	50.84 (0.5)	2.06 (0.9)	13.24 (0.8)	bdl	13.89 (0.6)	0.24 (8.5)
ND60	53.95 (0.4)	0.47 (2.4)	15.14 (0.6)	bdl	8.39 (0.8)	0.17 (8.3)
ND69	50.036 (0.8)	1.17 (1.0)	15.79 (1.2)	0.05 (15.7)	9.26 (2.3)	0.19 (11.6)
ND61	54.63 (1.1)	0.43 (3.2)	14.45 (0.7)	bdl	8.16 (1.7)	0.17 (15.9)
ND70	49.11 (0.3)	0.84 (2.4)	16.10 (0.3)	0.06 (8.6)	8.06 (0.8)	0.16 (14.1)
24.1	50.33 (1.1)	1.42 (1.6)	13.46 (0.7)	bdl	12.06 (1.0)	0.24 (17.0)
<u>Olivine</u>						
San Carlos	40.29 (1.1)	bdl	bdl	bdl	10.38 (0.9)	0.16 (8.5)
Pk Ol	41.42 (0.6)	bdl	bdl	bdl	4.87 (1.23)	0.16 (8.5)
<u>Pyroxene</u>						
Tan opx	57.53 (0.4)	0.04 (22.3)	0.11 (11.7)	bdl	6.34 (1.2)	0.26 (7.8)
PMR-53 cpx	54.28 (0.7)	0.37 (4.3)	2.85 (0.5)	0.16 (12.5)	7.25 (1.2)	0.19 (19.2)
KBH cpx	50.55 (0.4)	0.41 (2.2)	6.77 (0.4)	1.07 (3.8)	2.86 (1.8)	0.11 (31.5)
Cr diop	54.046 (0.5)	0.07 (13.1)	0.21 (5.8)	0.66 (2.3)	1.06 (2.6)	0.07 (20.2)
KBH opx	54.03 (0.6)	0.11 (9.8)	4.93 (1.3)	0.53 (3.7)	6.18 (1.8)	0.15 (13.5)

RSD are in parenthesis, based on n=7.

bdl = below detection limit.

FeO^t = total Fe

MgO	CaO	Na$_2$O	K$_2$O	NiO	Total
5.24 (1.1)	9.66 (0.8)	2.95 (2.8)	0.12 (15.2)	bdl	98.23
6.38 (0.8)	11.02 (0.5)	1.50 (5.0)	0.49 (5.1)	bdl	97.51
7.03 (1.2)	11.45 (1.8)	2.85 (2.9)	0.32 (4.4)	bdl	98.10
6.65 (0.9)	11.18 (0.7)	1.61 (6.4)	0.49 (5.1)	bdl	97.77
8.63 (0.8)	12.80 (0.9)	2.19 (4.6)	0.18 (9.8)	bdl	98.13
6.94 (0.9)	11.05 (0.8)	2.36 (19.0)	0.07 (19.6)	bdl	97.93
49.37 (0.3)	0.08 (12.9)	bdl	bdl	0.36 (5.7)	100.64
53.64 (0.1)	bdl	bdl	bdl	0.33 (6.4)	100.43
35.74 (0.2)	0.14 (3.4)	0.07 (0.0)	bdl	bdl	100.16
18.65 (0.6)	13.86 (0.4)	1.97 (5.0)	0.042 (29.6)	0.08 (14.5)	99.68
15.70 (0.2)	20.00 (0.3)	1.62 (3.4)	bdl	0.07 (8.6)	99.11
17.94 (0.5)	25.22 (0.1)	0.36 (11.3)	bdl	bdl	99.59
33.18 (0.4)	0.87 (2.5)	0.14 (18.0)	bdl	0.11 (6.4)	100.23

Table 2: Results of water analyses

Sample name	SHRIMP SI $^{16}OH/^{16}O$ (n=3)*	1σ standard deviation	reproducibility (%)	H_2O (ppm) SHRIMP SI calibrated†
Glasses				
36.4	1.51E-03	5.52E-06	0.37	7.73E+03
24.1	7.69E-04	1.18E-06	0.15	3.87E+03
ND60	2.74E-03	9.21E-06	0.34	1.42E+04
ND61	2.53E-03	3.56E-05	1.41	1.31E+04
ND69	2.47E-03	7.91E-07	0.03	1.27E+04
ND70	1.99E-03	2.08E-06	0.10	1.02E+04
Olivine				
San Carlos	4.35E-05	1.94E-06	4.46	81
Pk-olivine	8.10E-05	8.01E-07	0.99	277
Pyroxene				
KBH-1 opx	7.40E-05	1.20E-06	1.62	240
Tan opx	3.67E-05	1.98E-07	0.54	45
Rus Cr-diop	5.53E-05	2.16E-06	3.91	142
KBH cpx	1.01E-04	5.26E-06	5.21	381
PMR-53 cpx	8.01E-05	8.00E-07	1.00	272

*Analytical error per SHRIMP SI and Cameca analysis is typically less than 2 %.

† Calibration determined by single weighted line fit to all standard data (see text).

H_2O (ppm) contents of samples determined by the calibration curves of Hauri et al. 200

§ 1 standard deviation error on samples analysed in this study (n= >6). All other errors fo

References for H2O determination by (F) or (M) are as follows: (1) this study (2) Bell et al

Cameca 6F $^{16}OH/^{30}Si$ (n=4)*	1σ standard deviation	reproducibility (%)	H_2O (ppm) Cameca calibrated#	H_2O (ppm) FTIR (F) or Manometry (M)	1σ standard deviation§
1.89	1.00E-01	5.29	8.61E+03	7.40E+03	5.32E+02
0.85	6.92E-03	0.81	3.90E+03	3.10E+03	3.36E+02
3.41	6.16E-02	1.81	1.56E+04	1.61E+04	4.66E+02
3.06	7.43E-03	0.24	1.40E+04	1.39E+04	3.27E+02
3.14	5.14E-02	1.64	1.43E+04	1.34E+04	1.03E+02
2.47	4.72E-02	1.91	1.13E+04	9.98E+03	4.65E+01
4.08E-03	1.45E-03	35.54	15	10 (F)	2
7.37E-02	7.67E-04	1.04	338	337 (F)	41
5.59E-02	9.15E-04	1.64	216	217 (M)	14
1.03E-02	3.31E-04	3.21	40	33 (F)	4
2.59E-02	4.64E-04	1.79	100	125 (F)	14
8.49E-02	2.26E-03	2.66	498	530 (M)	
5.60E-02	2.89E-04	0.52	328	268(M)	7.5

)2 and Koga et al. 2003. Errors associated with this calibration is approximately 10 % for glass and 20 % for r

und in references.

. 1995 (3) Bell and Rossman 1992.

reproducibility (%)	References
7.19	1
10.85	1
2.89	1
2.35	1
0.77	1
0.47	1
20.00	1
12.17	1
6.45	2
12.12	1
11.20	1
	3
2.80	2

minerals

Table 3: Compilation of water contents of basaltic glasses determined by FTIR

Sample	thickness (µ)	±	density	3550	±
ND 60	82	4	2650	1.23	0.03
ND 61	92	4	2650	1.19	0.01
Nd 69	82	4	2650	1.03	0.03
ND 70	142	3	2650	1.32	0.03
36.4	142	3	2650	0.972	0.004
24.1	142	3	2650	0.402	0.007

*Water contents calculated with a density of 2650±50; e(3570) of 63.32±0.42 and e(1630) of 42.34±2.77 for Fe-bearing and

1630 ±		*H$_2$O (ppm)	±
0.154	0.004	1.61E+04	5.32E+02
0.145	0.003	1.39E+04	3.36E+02
0.076	0.002	1.34E+04	4.66E+02
0.055	0.003	9.98E+03	3.27E+02
0.03	0.0005	7.40E+03	1.03E+02
bdl		3.10E+03	4.65E+01

lesites from Mandaveille et al. 2002

1
2
3
4
5
6
7
8
9
10
11
12
13
14
15
16
17
18
19
20
21
22
23
24
25
26
27
28
29
30
31
32
33
34
35
36
37
38
39
40
41
42
43
44
45
46
47
48
49
50
51
52
53
54
55
56
57
58
59
60

Table 4. FTIR data of NAMs used in this study

Sample	Locality	IR integrated absorbance (cm^{-2})			A(total)	H_2O, Bell	H_2O, Ko
		a	b	g	cm^{-2}	ppm wt	ppm
Cr-diop	Russia	391 (20)	304 (15)	193 (10)	888	125 (14)	
Tan opx	Tanzania	138 (7)	75 (4)	282 (14)	495	33 (4)	
Pk-olivine	Pakistan	295 (15)	70 (4)	225 (11)	591	111 (14)	337
SC olivine	San Carlos	3 (1)	9 (1)	40 (4)	52	10 (2)	

Notes: integration range are 3750-3000 cm-1 for cpx, 3750-2800 cm-1 for opx and 3750-3300 for ol, "Bell" refers to calibrations by Bell et al. (1995) Bell et al. (2003) for pyroxenes and olivines respectively. "Kovács" referes to Kovács et al. (2010) for olivine.

1
2
3
4
5
6   ›vács
7   wt
8
9
10
11   (41)
12
13
14   ;) and
15
16
17
18
19
20
21
22
23
24
25
26
27
28
29
30
31
32
33
34
35
36
37
38
39
40
41
42
43
44
45
46
47
48
49
50
51
52
53
54
55
56
57
58
59
60